

Numerical Strategies for Mixed-Integer Optimization of Power-Split and Gear Selection in Hybrid Electric Vehicles

Downloaded from: https://research.chalmers.se, 2026-02-28 11:53 UTC

Citation for the original published paper (version of record):

Ganesan, A., Murgovski, N., Gros, S. (2023). Numerical Strategies for Mixed-Integer Optimization of Power-Split and Gear Selection in Hybrid
Electric Vehicles. IEEE Transactions on Intelligent Transportation Systems, 24(3): 3194-3210.
http://dx.doi.org/10.1109/TITS.2022.3229254

N.B. When citing this work, cite the original published paper.

© 2023 IEEE. Personal use of this material is permitted. Permission from IEEE must be obtained for all other uses, in any current or future media, including reprinting/republishing this material for advertising or promotional purposes, or reuse of any copyrighted component of this work in other works.

(article starts on next page)

Numerical Strategies for Mixed-Integer Optimization of Power-Split and Gear Selection in Hybrid Electric Vehicles

Anand Ganesan*,[1,3] Sébastien Gros[2] Nikolce Murgovski[3]

***Abstract*—This paper presents numerical strategies for a computationally efficient energy management system that co-optimizes the power split and gear selection of a hybrid electric vehicle (HEV). We formulate a mixed-integer optimal control problem (MIOCP) that is transcribed using multiple-shooting into a mixed-integer nonlinear program (MINLP) and then solved by nonlinear model predictive control. We present two different numerical strategies, a Selective Relaxation Approach (SRA), which decomposes the MINLP into several subproblems, and a Round-n-Search Approach (RSA), which is an enhancement of the known 'relax-n-round' strategy. Subsequently, the resulting algorithmic performance and optimality of the solution of the proposed strategies are analyzed against two benchmark strategies; one using rule-based gear selection, which is typically used in production vehicles, and the other using dynamic programming (DP), which provides a global optimum of a quantized version of the MINLP. The results show that both SRA and RSA enable about $3.6\,\%$ cost reduction compared to the rule-based strategy, while still being within $1\,\%$ of the DP solution. Moreover, for the case studied RSA takes about $35\,\%$ less mean computation time compared to SRA, while both SRA and RSA being about 99 times faster than DP. Furthermore, both SRA and RSA were able to overcome the infeasibilities encountered by a typical rounding strategy under different drive cycles. The results show the computational benefit of the proposed strategies, as well as the energy saving possibility of co-optimization strategies in which actuator dynamics are explicitly included.**

***Index Terms*—Mixed-Integer Nonlinear Optimal Control, Nonlinear Programming, Numerical Optimization, Hybrid Electric Vehicle, Energy Management, Nonlinear MPC, Optimal Torque-Split, Optimal Gear Selection.**

I. Introduction

In the field of optimal control of hybrid electric vehicles (HEVs), supervisory energy management control strategies have been the subject of very active research [1]–[6], in response to the exponential electrification of mobility [7]. A typical HEV has an over-actuated powertrain, i.e., it consists of an internal combustion engine (ICE) and one (or) more electrical machines (EM) to deliver the requested power. Depending on the powertrain configuration, these actuators are connected to the wheels via a multispeed transmission with a fixed set of gear ratios or a continuously variable transmission that can change seamlessly through a continuous range of gear ratios [3]. An over-actuated powertrain offers certain degrees of freedom to its control system to minimize fuel or energy consumption during a driving mission. Key control decisions that can be optimized are 1) the percentage allocation of total propulsive/braking demand to each of its actuators, referred to as power-split, torque-split or allocation [5], [6], 2) the choice of the most suitable gear to meet that demand (gear selection) [8]–[10], 3) the ICE ON-OFF decisions to avoid operating the ICE at inefficient speeds [10], [11], and 4) the vehicle speed variation around a reference set by a user or an autonomous system like in a cruise controller [3], [9], [12], [13].

Among the control decisions listed above, gear selection and ICE on-off are discrete decision variables, whereas the other decisions are continuous. Hence, when any or both of the discrete variable(s) is to be co-optimized either with the actuator power-split or vehicle velocity or both, it most often leads to a Mixed-Integer Nonlinear Programming (MINLP) problem [8], [9], [14]. Such an MINLP needs to be solved in real-time in an online controller to enable minimization of fuel or energy consumption in an HEV. But mixed-integer problems are generally NP hard (nondeterministic polynomial-time hardness), i.e., any algorithm that guarantees to find the global solution to such problems suffers from non-polynomial worst-case time complexity (unless P=NP) [15]. Hence, numerical strategies that can find 'nearly-optimal' solution(s) for an MINLP and yet have less real-time computational demand, are vital for online (or embedded) implementation of fuel or energy minimizing co-optimization strategies in HEVs.

A. Global Algorithms for Mixed-Integer (MI) Problems

The widely used method to solve MI problems offline is Dynamic Programming (DP) [4], [11], [16], [17], which is based on the Bellman principle of optimality [18]. Though DP can find the global optimum and handle non-convex nonlinear problems effectively, the optimality of its solution can be guaranteed only within the discretization accuracy of its states and controls. Other direct methods capable of solving MI problems to optimality are integer enumeration, branch-and-bound, cutting planes, piecewise linear approximations, etc., [19]–[22]. All these methods are computationally too expensive due to the combinatorial nature of MI problems and suffer from large run-time variations. Although these computational and run-time aspects are less favorable, main obstacles for the real-time implementation of these direct methods are the limited memory and computational capacity of the embedded or online control hardware in HEVs.

This work is funded by the *Sweden´s Innovation Agency (Vinnova)*.

* Corresponding author. Email: anand.ganesan@volvocars.com.
[1] *R&D, Volvo Car Corporation*, Gothenburg, Sweden.
[2] *Department of Engineering Cybernetics, Norwegian University of Science and Technology*, Trondheim, Norway. Email: sebastien.gros@ntnu.no.
[3] *Department of Electrical Engineering, Chalmers University of Technology*, Gothenburg, Sweden. Email: nikolce.murgovski@chalmers.se.

Nomenclature			
s, t	Coordinates: Spatial, and temporal.	η_γ, η_{ig}	Efficiencies: Transmission, and ignition angle.
v, ω	Velocities: Longitudinal, and angular.	$(\cdot)$	A function dependant on several elements.
$a_0, .., a_8$	Coefficients of ICE fuel power consumption model.	$(\cdot)^*$	Optimum value.
$b_0, .., b_8$	Coefficients of ISG power consumption model.	$(\cdot)^+$	Value at next discrete time step.
$c_0, .., c_3$	Coefficients describing the bounds of ICE power.	$(\cdot)^{\min}, (\cdot)^{\max}$	Minimum value, and maximum value.
$c_{\rm ad}, c_{\rm rr}$	Coefficients of Air drag, and rolling resistance.	$\dot{(\cdot)}$	First order temporal derivative.
$d_1, .., d_6$	Coefficients describing the bounds of ISG power.	$\hat{(\cdot)}$	Initial estimate (guess) of a variable.
$e_0, .., e_5$	Coefficients of gear ratio model.	$\tilde{(\cdot)}$	States, controls, and parameters of an MINLP.
$F_{\rm pt,brk}^{\max}$	Maximum breaking capacity of the powertrain.	x, u, θ	State, control, and parameter vectors.
F, r, J	Wheel force, radius, and rotational Inertial.	$\Gamma, \mathbf{U}$	Discrete feasible sets: Gear, and gear shift control.
α, g, τ	Road slope, gravitational constant, and time constant.	f, h	A function of one or more elements.
$A_{\rm fa}, \rho_{\rm air}$	Vehicle frontal surface area, and air density.	$\lambda_{\rm b}, \lambda_{\rm sr}$	Battery co-state factor, and stoichiometric ratio.
$m, m_{\rm e}$	Net laden mass and equivalent mass of vehicle.	ϕ, L	Cost functions of an MPC: Stage and terminal costs.
P	Power consumed or delivered.	$t_{\rm h}, N$	Prediction horizon: Continuous and discrete time domains.
$P_{\rm ice}, \gamma$	States: ICE power delivery, and gear.	W, w_γ	Gear shift penalty function, and its penalty factor.
$P_{\rm ice,req}$	Controls: ICE power request, and ISG power delivery.	ζ, j	MPC update instance: Continuous, and discrete time domains.
u_γ, d_γ	Binary Controls: Function, and gear shift decision.	k	Discrete time instance of an MPC prediction window.
$U_{\rm ocv}$	Open circuit voltage of the battery.	$(k \mid j)$	A vector element at current instant j and prediction instant k.
$R_{\rm b}$	Internal resistance of battery.	Δt	Fixed sampling or discretization interval.
$R_{\rm pa}$	Polynomial approximation of gear ratio.	$t_0, t_{\rm f}$	Start time, and final time of the driving mission.
$R, R_{\rm dg}$	Ratios: Current gear, and differential gear.	w.r.t.	Abbreviation: With respect to.
ADMM	Alternating Direction Method of Multipliers	**Subscripts**	
BMS	Battery Management System.	l	Set describing the indices of the binary variable, d_γ.
ECM, MCU	Engine Control Module, and Motor Control Unit.	r	A variable or a vector of variables in an MINLP whose integral constraint is relaxed.
ICE	Internal Combustion Engine.	$\rm brk, s$	Powertrain components: Friction brake, and drive shaft.
ISG, MPC	Integrated Starter Generator, and Model Predictive Control.	$\rm cl, whl$	Powertrain components: Transmission clutch, and wheel.
AMT	Automated Manual Transmission.	$\rm dm, aux$	Power demanded: Primary load, and auxiliary load.
TCM	Transmission Control Module.	$\rm ech, el$	Energy domain: Electro-chemical, and electrical.
MIOCP	Mixed-Integer Optimal Control Problem	$\rm f, b$	Energy Sources: Fuel, and battery.
MINLP	Mixed-Integer Nonlinear Problem	$\rm fes, ss$	Feasible value, and steady-state value.
SCC	Supervisory Co-Optimization Controller.	$\rm red$	Reduced feasible region or set.
SOE	State-of-Energy of a battery pack.	$\rm req, rgn$	Request (control signal), and regeneration.
NRMSE	Normalized Root Mean Squared Error.	$\rm up, dn$	Indices of binary variable, d_γ: Up shift, and down shift.

B. Heuristics for MINLPs

Several methods have been proposed in recent years that could approximately solve the MI problem to an acceptable level of suboptimality and still remain computationally efficient. For example, multiphase and parameteric methods were proposed in [12], [23]–[25], hierarchical methods in [10], [26], integer relaxation, decomposition and reformulation methods in [27]–[29], and DP-based or other offline approaches in [30], [31]. Since, this article focuses on real-time capable solution approaches for the MI problem considered, we present below some of the closely related work in this context.

Relaxation strategy in which the integer constraint is relaxed to obtain an NLP, is a typical choice to solve such MI problems. For example, strategies like relax-and-round or 'rounding' strategy, in which the integer feasible set is relaxed to its convex hull, was found to be an effective method in [32], [33]. It was shown in [32] that the method may not converge to an integer feasible solution for some cases, as is expected for heuristic methods. Another relaxation strategy labeled 'outer convexification', proposed in [32] can guarantee feasibility and showed promising real-time capabilities when applied in MPC-based cruise controller. Moreover, this 'outer convexification' strategy was used to solve the MI problem of optimizing the torque-split, gear choice and ICE on/off in a distributed control framework [8], but the optimality gap of the results was not analyzed.

An alternate method proposed in recent works addresses such MI problems using a distributed approach which exploits the additional resources in control architectures, referred as 'hierarchical' or 'multi-layered' or 'sequential' or 'distributed' control frameworks. In such an approach, the continuous and discrete decisions are decomposed as two subproblems and addressed either separately in different layers (or different entities in the same layer) of the architecture or iterated by passing on the decisions between the layers (or entities). For example, quadratic programming (QP), convex programming, etc. were used to solve real-valued decisions, while a rule-based (non-optimal) or DP (computationally heavy) strategy was used for the discrete decisions in [9]–[11], [13]. Such a distributed approach is real-time capable but it quite often converges to a worse local optimum compared to a centralized approach [9], [34]. The iterative schemes proposed in [9], [35] showed that the optimality of such a distributed approach can be improved by iteratively passing the suboptimal decision values from one layer to the other layer(s).

Recently, other heuristic methods have shown promising real-time capabilities. In [36] the continuous relaxed version of MINLP is reformulated so that the solution of the reformulated NLP is a local minimizer of the original MINLP in most cases. In [36] the authors focused on co-optimizing vehicle speed and gear ratio, whereas the power-split decision was not considered. Furthermore, the mean computational time required to solve the MINLP was in the range of $0.6\,\mathrm{s} - 1.9\,\mathrm{s}$ in [36], which needs to be further improved for real-time implementation in HEVs. In [37], a heuristic gear search strategy was proposed, which searches the neighboring gears of a reference gear trajectory (derived from a rule-based gear map) to find a better solution. Although the strategy showed promising results, the computational demand of the strategy was not analyzed in [37]. Other strategies include an approach based on Reinforcement Learning (RL) for stochastic problems [38] and an alternating direction method of multipliers

(ADMM) based approach for deterministic cases [15], [39]. The RL based approach in [38] is yet to be applied to the HEV MINLP whereas the strategies proposed in [15], [39] co-optimize only the binary decision 'ICE on-off' and power-split, but not the gear selection.

Besides the difficulty in solving MI problems faster to enable real-time implementation, in the existing literature on energy management of hybrid electric vehicles, a standard approach to model the energy conversion dynamics of the powertrain actuators is to approximate them as steady-state efficiency maps [1], [3], [8], [32]. However, in [40]–[42] it was shown that such approximations often result in lower energy savings in an optimal torque-split controller and that the savings can be improved by considering actuator dynamics.

C. Contributions of the Article

In this article, we focus on the centralized mixed-integer optimal control problem (MIOCP) of optimizing the power-split and the gear choice to minimize energy consumption in HEVs. Although such optimization strategies are not novel on their own [8], [32], [39], [41], they have not been previously applied to an HEV energy management in which engine dynamics is also considered. We show that considering the engine dynamics with the proposed mixed-integer control strategies provides a considerable benefit to fuel economy. Furthermore, we show conceptually that proposed relaxation strategies can find 'nearly-optimal' solutions for the MIOCPs posed by hybrid electric powertrains and yet remain numerically sufficiently effective to ensure the real-time capability of the algorithm for the considered application.

In particular, the main contributions of the article in the context of the considered application are: 1) We show that explicit inclusion of actuator dynamics in the energy management problem of co-optimizing the power-split and gear selection enables realization of higher energy savings in an HEV, by exploiting the predictive capabilities of the MPC framework; 2) We propose relaxations and reformulations to reduce computational demand while solving the MIOCP in real time; 3) We propose two intuitive numerical solution strategies, the Selective Relaxation Approach (SRA) and the Round-n-Search Approach (RSA), to approximately solve the MINLP (discretized MIOCP) without any feasibility issues under different driving missions; 4) We analyze the performance and computational demand of the proposed strategies against benchmark strategies based on rule-based gear selection and DP; 5) We quantity the optimality gap of the solutions of the proposed strategies by comparing against the DP solution, which we regard as the closest solution to the MI optimum for the original MIOCP.

Furthermore, the results show the computational benefit of the proposed strategies to solve MI problems efficiently and to remain feasible for implementation in a core computing unit onboard an electrified vehicle. These proposed mixed-integer solution strategies can be extended and integrated into a computer software in future intelligent transportation systems to solve similar MI problems, including charge point selection for electric vehicles, fleet management, intelligent traffic management, and a wide range of other mobility solutions.

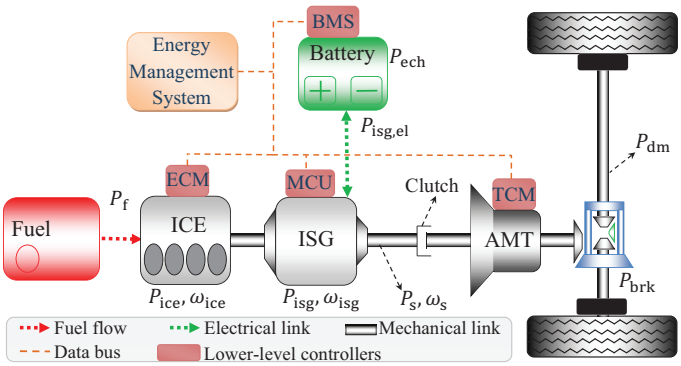


Fig. 1: The considered parallel HEV powertrain consists of an ICE and an ISG connected to the wheels via an 8-speed auto-transmission, where P_{brk} is the braking power demanded. The Energy Management System hosts the proposed supervisory co-optimization controller (SCC) which sends optimal references to each of the lower-level controllers.

D. Article Outline

In Section II, control-oriented model of the considered powertrain is described along with its decision variables, parameters, and constraints. Section III introduces the proposed supervisory co-optimization controller with its architecture, assumptions, and problem formulation. In Section IV, model and constraint relaxations are proposed to improve the numerical efficiency of the solution process, before transcribing the reformulated problem as a finite-dimensional MINLP. Section V presents the numerical strategies proposed to approximately solve MINLP. Section VI briefs the benchmark controllers implemented for comparison. Finally, the relative performance and energy savings of the proposed strategies are discussed in Section VII, followed by the conclusion in Section VIII.

II. Control-Oriented Modelling

In this section, control-oriented models of different components and sub-systems in the parallel HEV powertrain used for this study are described. The considered powertrain, as shown in Fig. 1, has an internal combustion engine (ICE), an integrated starter generator (ISG), an 8-speed auto-transmission unit, a clutch, a battery, a differential along with other driveline components, wheels, and low-level controllers for some powertrain components.

A. Vehicle Dynamics: Power Demand at Wheels

Using a point mass representation, the longitudinal vehicle dynamics can be modelled as in [3] as

$$\begin{aligned}\dot{v}(t) m_{\text{e}}(\cdot) = F(t) + F_{\text{brk}}(t) - \frac{c_{\text{ad}} A_{\text{fa}} \rho_{\text{air}} v^2(t)}{2} \\ - mg\left(\sin\alpha(s) + c_{\text{rr}} \cos\alpha(s)\right),\end{aligned} \tag{1}$$

where c_{ad} is the aerodynamic drag coefficient, A_{fa} is the vehicle frontal surface area, ρ_{air} is the air density, s is the travelled distance, m is the vehicle mass, α is the road slope, c_{rr} is the rolling resistance coefficient, F is the traction force of the ICE and ISG, F_{brk} is the force dissipated within the

friction brakes, v is the linear velocity of the vehicle and the equivalent mass $m_{\rm e}$ is computed as [11], [43],

$$m_{\rm e} = m + \frac{J_{\rm wh1} + x_{\rm cl}(t)(J_{\rm ice} + J_{\rm isg})(R(\gamma)R_{\rm dg})^2}{r_{\rm wh1}^2}, \quad (2)$$

where $x_{\rm cl}$ is the transmission clutch engagement decision, $R(\gamma)$ is the ratio of current gear γ, $R_{\rm dg}$ is the fixed ratio of differential gear, $r_{\rm whl}$ is the wheel radius, and $J_{\rm ice}$, $J_{\rm isg}$ and $J_{\rm whl}$ are the inertia of the ICE, ISG, and all other powertrain components lumped together to reflect at wheels, respectively. If the trajectories of $v(t), \alpha(t)$ are known a priori, then using (1) and assuming that the brake controller always ensures $F_{\rm brk} = 0$ when $F > 0$ and $F_{\rm brk} < 0$ otherwise, the power demand at the wheels can be calculated a priori for $\forall t$ as

$$P_{\rm dm}(t) = \begin{cases} F(t)v(t), & F(t) \geq F^{\max}_{\rm pt,brk}(t), \\ (F(t) - F_{\rm brk}(t))\, v(t), & F(t) < F^{\max}_{\rm pt,brk}(t), \end{cases} \quad (3)$$

where, the maximum capacity of the powertrain (depends on ICE braking and ISG regeneration capacities) is expressed as

$$F^{\max}_{\rm pt,brk} = \max(F_{\rm ice,brk}(v, \gamma_{\rm fes}, t) + F_{\rm isg,rgn}(v, \gamma_{\rm fes}, t)), \quad (4)$$

and the trajectory of sets of all feasible gears, $\gamma_{\rm fes}(t)$, is

$$\gamma_{\rm fes} = \{\gamma \mid \gamma \in \{\gamma^{\min}(v(t), F(t)), \gamma^{\max}(v(t), F(t))\}\}. \quad (5)$$

B. Transmission and Drivetrain Components

Assuming a clutch lock-up , i.e., $x_{\rm cl}(t) = 1 \mid \forall t$, power-transfer through the auto-transmission (actuated by transmission control module, TCM) and other drivetrain components (differential, axle shafts, and joints) can be modelled as

$$P_{\rm s}(t) = \begin{cases} P_{\rm dm}(t)/\eta_\gamma(\gamma), & P_{\rm dm}(t) > 0, \\ P_{\rm dm}(t)\eta_\gamma(\gamma), & P_{\rm dm}(t) \leq 0, \end{cases} \quad (6)$$

where $\eta_\gamma(\gamma)$ is the net efficiency of current gear γ and a fixed differential gear. Assuming a constant value for $\eta_\gamma(\gamma)$, the demand at the shaft $P_{\rm s}(t)$ can be precalculated $\forall t$, thus reducing (6) to a simple power balance equation,

$$P_{\rm ice}(t) + P_{\rm isg}(t) = P_{\rm s}(t), \quad (7)$$

where $P_{\rm isg}$ is the ISG power delivery and $P_{\rm ice}$ is the power delivered by the ICE [11]. The transmission gear dynamics is represented as a discrete-time model with an integer gear shift control input, $u_\gamma \in \mathbf{U}$, as

$$\gamma^+(t) = \gamma(t) + u_\gamma(t), \quad (8)$$

$$u_\gamma(t) \in \mathbf{U} = \{u_\gamma^{\min}, \ldots, -1, 0, 1, \ldots, u_\gamma^{\max}\},\ \forall t, \quad (9)$$

$$\gamma(t) \in \Gamma = \{0, 1, .., \gamma^{\max}\},\ \forall t, \quad (10)$$

where Γ and $\mathbf{U}$ refer to the discrete sets for the state and the control, respectively. Then the ratio of current gear, $R(\gamma)$, and the angular velocity of the drive shaft, $\omega_{\rm s}$, can be denoted as

$$R = f(\gamma)_{\gamma \in \Gamma}, \quad (11)$$

$$\omega_{\rm s}(t) = \begin{cases} \omega_{\rm s}^{\min}, & \gamma(t) = 0, \\ v(t)R(\gamma)R_{\rm dg}/r_{\rm whl}, & \gamma(t) \geq 1, \end{cases} \quad (12)$$

$$\omega_{\rm s}(t) \in [\omega_{\rm s}^{\min}, \omega_{\rm s}^{\max}],\ \forall t, \quad (13)$$

where $\omega_{\rm s}^{\min}$ refers to the idle speed of the engine. Furthermore, as both the actuators (ICE and ISG) are connected to the same drive shaft, their angular velocities are the same.

C. Internal Combustion Engine (ICE) Dynamics

Modelling the ICE dynamics accurately is quite challenging due to the highly complex nonlinear interactions of its subsystems. However, control-oriented modelling of both transient and steady-state behaviours of an actuator-controller closed-loop system is tractable [3], [40]. So, in this study, the dynamics of the supercharged gasoline ICE with its integrated engine control module (ECM) is modelled as a closed-loop actuator-controller system as proposed in [40]. The ECM exploits torque compensation mechanisms to ensure the delivery of the requested ICE performance, as long as the request $P_{\rm ice,req}$ is within its bounds;

$$P^{\min}_{\rm ice}(\omega_{\rm ice}) \leq P_{\rm ice,req}(t) \leq P^{\max}_{\rm ice}(\omega_{\rm ice}). \quad (14)$$

1) Dynamic Response Model: The simplified dynamic model of the gasoline ICE proposed in [40] can be transformed to its equivalent approximate representation in the power domain, with a suitable response time constant $\tau_{\rm ice}$, as follows

$$\dot{P}_{\rm ice}(t) = (\eta_{\rm ig}(t)P_{\rm ice,req}(t) - P_{\rm ice}(t))/\tau_{\rm ice}, \quad (15)$$

$$P_{\rm ice}(t) \in [P^{\min}_{\rm ice}(\omega_{\rm ice}(t)), P^{\max}_{\rm ice}(\omega_{\rm ice}(t))], \quad (16)$$

where $\eta_{\rm ig}$ refers to the ignition efficiency. The speed-dependant bounds of the ICE power in (14) and (16) are approximated as an affine function,

$$P^{\min}_{\rm ice} = c_1\omega_{\rm ice} + c_0, \quad P^{\max}_{\rm ice} = c_3\omega_{\rm ice} + c_2. \quad (17)$$

The model in (17) has a root mean squared error (NRMSE) of about $2\,\% - 2.6\,\%$ (normalized w.r.t. the maximum value of data) within the speed range of interest, as shown in Fig. 2.

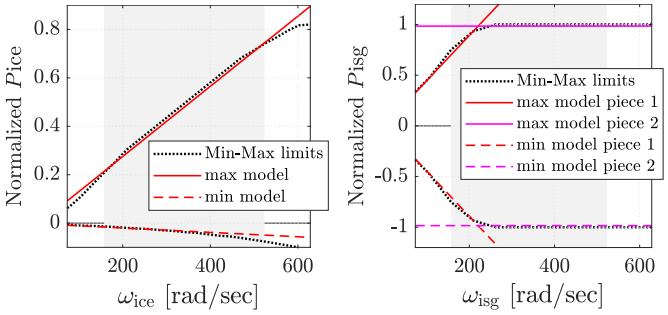
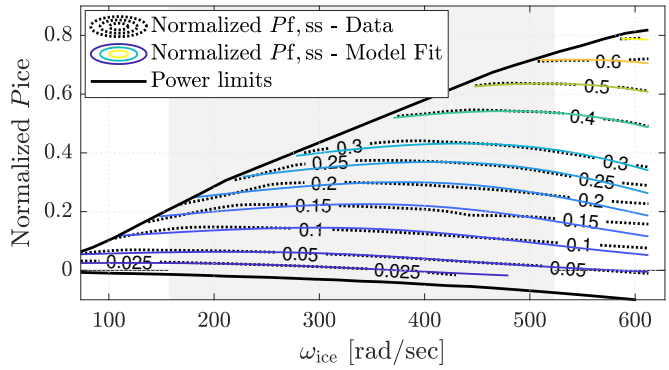


Fig. 2: Left figure shows the min-max limits of the ICE power. Its affine models, $P^{\min}_{\rm ice}$ (dashed line) and $P^{\max}_{\rm ice}$ (solid line), have an NRMSE of about $2\,\%$ and $2.6\,\%$, respectively in the operating speed range of $1500\,$rpm to $5000\,$rpm (grey shaded region). Right figure shows the min-max limits of the ISG power. Its piece-wise affine models (Pieces: 1 and 2), $P^{\min}_{\rm isg}$ (dashed line) and $P^{\max}_{\rm isg}$ (solid line), exhibit an NRMSE of about $2.1\,\%$ each in the grey shaded region. In both the figures, the power in y-axis and the NRMSE values are normalized w.r.t. the maximum value of their respective measurements.

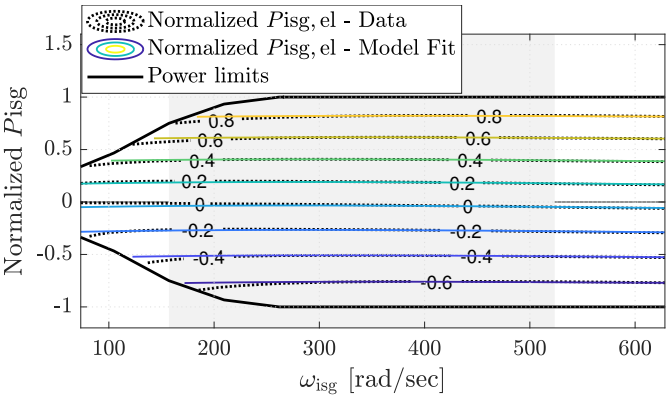
2) Dynamic Fuel Consumption Model: The static map of the rate of gasoline energy consumption of ICE under steady state ($P_{\rm f,ss}$) is approximated as a nonlinear model as follows

$$P_{\rm f,ss} = a_0 + a_1\omega_{\rm ice} + a_2\omega^2_{\rm ice} + a_3P_{\rm ice} + a_4P^2_{\rm ice} + a_5P^3_{\rm ice} + \omega_{\rm ice}P_{\rm ice}(a_6\omega_{\rm ice} + a_7 + a_8P_{\rm ice}). \quad (18)$$

This model has an NRMSE of $<0.5\,\%$ (normalized w.r.t. the maximum value of data) within the operating speed range, as shown in Fig. 3(a). The dynamic energy consumption rate



(a) Normalized values of the measured (dotted line) and the estimated (solid line) gasoline consumption of the ICE, $P_{\mathrm{f,ss}}$, illustrated as contour lines.



(b) Normalized values of the measured (dotted line) and the estimated (solid line) electrical power consumption of the ISG, $P_{\mathrm{isg,el}}$, illustrated as contours.

Fig. 3: Gasoline consumption of the ICE and energy consumption of the ISG. Both models exhibit a good fit, with a NRMSE of $<0.5\,\%$ in the operating speed range of interest, $1500\,\mathrm{rpm}$ to $5000\,\mathrm{rpm}$ (shaded region in grey). In both figures, the power in y-axis, the consumption contours and the NRMSE values are normalized w.r.t. the maximum value of their respective measurements.

$P_{\mathrm{f}}(t)$ can then be estimated using $P_{\mathrm{f,ss}}$, ignition efficiency η_{ig}, the dynamic power response from (15), and the stoichiometric ratio λ_{sr}, as [40]

$$P_{\mathrm{f}}(t) = \frac{P_{\mathrm{f,ss}}\left(\omega_{\mathrm{ice}}(t), P_{\mathrm{ice}}(t)/\eta_{\mathrm{ig}}(t)\right)}{\lambda_{\mathrm{sr}}(t)}. \tag{19}$$

D. Integrated Starter Generator (ISG) and Battery Model

The electrical power transferred via ISG ($P_{\mathrm{isg,el}}$) is represented by a nonlinear model and the bounds of the ISG mechanical power delivery (P_{isg}) are approximated by piecewise affine functions as

$$\begin{aligned} P_{\mathrm{isg,el}} &= b_0 + b_1\omega_{\mathrm{isg}} + b_2\omega_{\mathrm{isg}}^2 + b_3 P_{\mathrm{isg}} + b_4 P_{\mathrm{isg}}^2 \\ &\quad + b_5\omega_{\mathrm{isg}}^3 + \omega_{\mathrm{isg}} P_{\mathrm{isg}}(b_6\omega_{\mathrm{isg}} + b_7 + b_8 P_{\mathrm{isg}}), \end{aligned} \tag{20}$$

$$P_{\mathrm{isg}}(t) \in [P_{\mathrm{isg}}^{\min}(t), P_{\mathrm{isg}}^{\max}(t)], \tag{21}$$

$$P_{\mathrm{isg}}^{\min} = \max\{d_3\omega_{isg} + d_2,\ d_1\}, \tag{22}$$

$$P_{\mathrm{isg}}^{\max} = \min\{d_6\omega_{isg} + d_5,\ d_4\}, \tag{23}$$

where ω_{isg} is the ISG angular velocity. Figs. 2 and 3(b) show that the models representing the bounds and power consumption of the ISG have a good fit with an NRMSE of

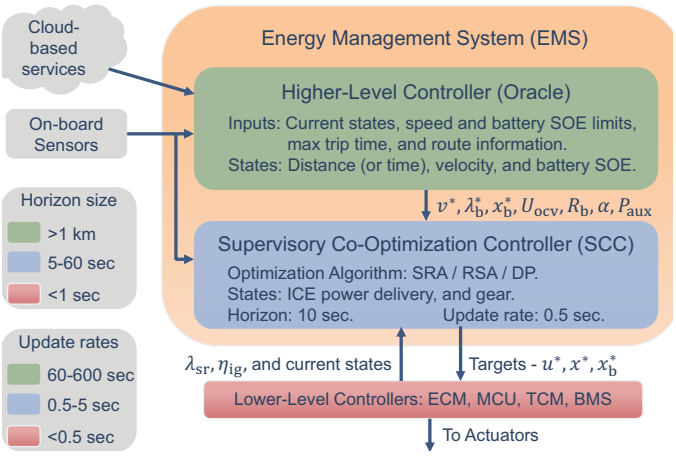


Fig. 4: The Hierarchical Control Framework with the interfaces for the proposed Supervisory Co-optimization Controller (SCC). Each layer operates with different time scales, prediction horizons, and model abstractions. The higher-level controller feeds the optimal trajectories of states and corresponding dual variables as state references and co-state factors to the SCC. The SCC then optimizes the power-split and gear trajectories, and orchestrates the lower-level controllers by feeding them with optimal control targets.

$\sim 2.1\,\%$ and $<0.5\,\%$, respectively, in the operating speed range. The rate of energy consumption from the battery is given by

$$\begin{aligned} P_{\mathrm{ech}}(t) &= P_{\mathrm{isg,el}}(\omega_{\mathrm{isg}}(t), P_{\mathrm{isg}}(t)) + P_{\mathrm{aux}}(t) \\ &\quad + R_{\mathrm{b}}(x_{\mathrm{b}}(t)) P_{\mathrm{ech}}^2(t)/U_{\mathrm{ocv}}^2(x_{\mathrm{b}}(t)), \end{aligned} \tag{24}$$

where x_{b} is the state-of-energy (SOE) and P_{aux} is the auxiliary power. Since we optimize power-split instead of torque-split in this work, the lumped internal resistance R_{b} and the open circuit voltage U_{ocv} of the battery are modelled as static functions of SOE (based on experimental data similar to [44]) instead of battery state-of-charge (SOC) to avoid the need to measure or estimate battery current in the HEV. The algebraic solution for (24) is [40]

$$\begin{aligned} P_{\mathrm{ech}}(t) &= \frac{U_{\mathrm{ocv}}^2(x_{\mathrm{b}})}{2R_{\mathrm{b}}(x_{\mathrm{b}})} \\ &\quad - U_{\mathrm{ocv}}(x_{\mathrm{b}}) \frac{\sqrt{U_{\mathrm{ocv}}^2(x_{\mathrm{b}}) - 4R_{\mathrm{b}}(x_{\mathrm{b}}) P_{\mathrm{isg,el}}(t)}}{2R_{\mathrm{b}}(x_{\mathrm{b}})}. \end{aligned} \tag{25}$$

III. Optimal Control Problem Formulation

In this section, a supervisory control strategy is proposed to minimize the energy consumption of the considered parallel HEV powertrain by co-optimizing the power-split and the gear selection. The ICE on-off decision, is not considered in this work due to the absence of clutch between the ICE and ISG in the powertrain configuration considered, see Fig. 1. First, we describe the hierarchical control framework and its assumptions considered in this study. Then we formulate the energy management problem of the proposed controller as a mixed-integer optimal control problem (MIOCP).

A. Supervisory Co-Optimization Controller (SCC)

We consider a hierarchical control framework as shown in Fig. 4, where the controllers at different levels operate with distinct time scales, prediction horizons, update rates

and model abstractions. In this study, we focus only on the supervisory co-optimization controller (SCC) that controls different lower-level controllers by setting optimal targets. Therefore, we only describe the SCC and its interface with the controllers in other layers rather than describing the controllers at higher and lower levels in detail.

In this study, it is assumed that the higher-level controller (the oracle in Fig. 4) receives information of the road slope $\alpha(t)$, speed limits, and traffic data from cloud-based navigation service providers for both the current and future road segments of a chosen route. Based on these predicted information, the oracle optimizes the vehicle speed $v(t)$, the battery SOE $x_{\mathrm{b}}^*(t)$ and co-state $\lambda_{\mathrm{b}}^*(t)$ to minimize energy consumption for the entire mission or over longer horizon with slower update rate relative to SCC. This means that the higher-level controller ensures the terminal constraints on trip time, battery SOE, and distance are met. Since, such an optimization is performed over long horizons, vehicle and powertrain models of higher abstraction are used to ensure the problem is tractable. These optimized predictions of speed and battery references are then provided to the SCC, along with the internal battery parameters, $U_{\mathrm{ocv}}(x_{\mathrm{b}}^*)$ and $R_{\mathrm{b}}(x_{\mathrm{b}}^*)$. Meanwhile, lower-level controllers transmit the current estimates of ignition efficiency $\eta_{\mathrm{ig}}(t)$, stoichiometric ratio $\lambda_{\mathrm{sr}}(t)$, and states $P_{\mathrm{ice}}(t)$ and $\gamma(t)$ to the SCC for every MPC iterate. Among these, parameters $\eta_{\mathrm{ig}}(t)$ and $\lambda_{\mathrm{sr}}(t)$ are assumed to be constant within a single MPC window. Then, the SCC uses these information to minimize energy consumption by including models of actuator dynamics and co-optimizing the future trajectories of power-split ($P_{\mathrm{ice}}(t)$ and $P_{\mathrm{isg}}(t)$) and gear selection ($\gamma(t)$) in a shorter horizon with faster update rate relative to the oracle. These optimal trajectories of power-split and gear selection are used as optimal control targets by lower-level controllers to control their respective actuators. Representative values of horizon size and update rates are provided in Fig. 4. Furthermore, we assume a perfect prediction case to calculate the demand trajectories and to optimize the decision variables subsequently.

Remark 1 (Optimization of co-state)**.** *As stated above, the optimal co-state (equivalence factor) λ_{b}^* that relates the cost of battery energy to fuel consumption is considered to be optimized by the oracle. This co-state is a time-varying parameter for the SCC, which is explicitly shown in the parameter vector $\theta(t)$ in* (38c)*. The oracle could use methods based on Pontryagin minimum principle which could ensure optimality of the costate [6], [45]. Consequently, incases where the battery limits could become active during a driving mission, the co-state could typically be optimized iteratively or using other adaptive or predictive methods based on the equivalent consumption minimization strategy (ECMS) [6], [46].*

Remark 2 (SOE dependence of battery parameters)**.** *The variation in internal battery parameters, $U_{\mathrm{ocv}}(x_{\mathrm{b}})$ and $R_{\mathrm{b}}(x_{\mathrm{b}})$, is negligible for small SOE deviations in an HEV [6]. Hence, when the considered prediction horizon t_{h} is significantly shorter than the fixed final time t_{f}, i.e., $t_{\mathrm{h}} \ll t_{\mathrm{f}}$, it is reasonable to neglect the SOE dependence in* (25)*, and assume that U_{ocv} and R_{b} remain approximately constant for a prediction horizon of a few seconds [6]. However, these constants are updated each time the prediction horizon moves one step forward in time t. In addition, the value of these constants follows the SOE trajectory optimized by the oracle.*

B. Mixed-Integer Optimal Control Problem Formulation

The objective of the SCC is to minimize the energy consumption of the HEV powertrain over the control inputs u_γ (discrete) and $P_{\mathrm{ice,req}}$ (continuous) while adhering to the state dynamics $x(t)$ defined in (8) and (15), for a specific horizon, $t \in [t_0, t_{\mathrm{h}}]$. This MIOCP objective is stated as a Hamiltonian,

$$H_{\mathrm{p}} = P_{\mathrm{f}}(x, u, \theta, t) + \lambda_{\mathrm{b}}^*(t) P_{\mathrm{ech}}(x, u, \theta, t), \tag{26}$$

where the first and second terms aggregate gasoline fuel and battery energy consumptions, respectively. While x, u, and θ refer to the trajectories of the state, control, and parameter vectors, respectively.

Furthermore, frequent gear changes are an unwanted side effect when the gear is optimized to minimize energy or fuel consumption [9], [32], [36]. To penalize this effect, an additional cost is added to the objective as

$$W = w_\gamma(|u_\gamma(t)|), \tag{27}$$

where w_γ is an adjustable weight for penalizing gear changes and the gear shift control input u_γ is a function whose value is non-zero only at instances of gear change and zero otherwise [9]. It will be described in details in Section IV-F after the discretization is performed. The energy management problem to be solved by the SCC can then be formulated as an MIOCP,

$$\min_{x,u} \int_{t_0}^{t_{\mathrm{h}}} \{H_{\mathrm{p}}(x, u, \theta, t) + W(u, t)\}\, dt \tag{28a}$$

$$\text{s.t.} \quad (7) \text{ to } (10), (14) \text{ to } (16) \text{ and } (21). \tag{28b}$$

IV. Reformulations for numerical efficiency

In this section, we describe numerically efficient reformulation of the transmission models in (8) to (11), to reduce the integer complexity in (28). In addition, we relax (7) to avoid infeasibility due to resource constraints. Finally, we transcribe the reformulated energy management problem into an MINLP.

A. Reducing the Size of Feasible Set of Gears

The TCM ensures the dependency of the transmission clutch engagement decision (x_{cl}) on the gear state (γ) as

$$x_{\mathrm{cl}} = \begin{cases} 1 \text{ (engaged)}, & \gamma \geq 1, v \geq \omega_{\mathrm{s}}^{\min} r_{\mathrm{whl}}, \\ 0 \text{ (disengaged)}, & \gamma < 1, v < \omega_{\mathrm{s}}^{\min} r_{\mathrm{whl}}. \end{cases} \tag{29}$$

Consequently, the neutral gear denoted by $\gamma = 0$ can then be removed from (10) to reduce the set of feasible gears as

$$\Gamma_{\mathrm{red}} = \Gamma \setminus \{0\}. \tag{30}$$

Using this reduced set Γ_{red} in problem (28), instead of the set described in (10), reduces the integer search space and, in turn, the computational demand to solve (28).

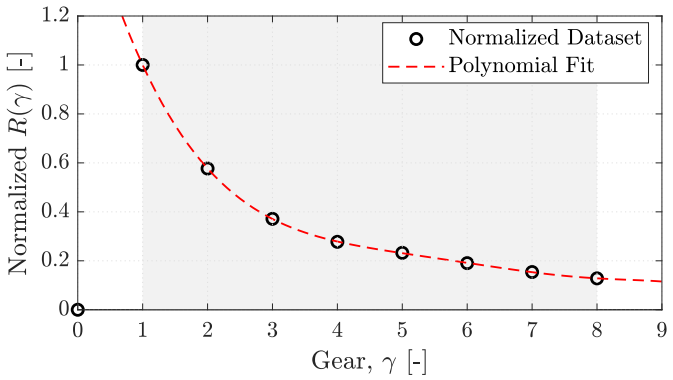


Fig. 5: Normalized gear ratio as function of gear. The black circles represent the discrete data-set whereas the dashed-line shows the polynomial approximation of ratio over $\gamma \in \Gamma_{\text{red}}$. The grey shaded region shows the reduced operating gear range Γ_{red} considered for the reformulation of MIOCP.

B. Ratio Model as a Continuous Function of Gears

The integer complexity of the ratio model is reduced by expressing it as a continuous function instead of a discrete function. Fig. 5 shows the fit of such a ratio model R_{pa}, a polynomial approximation of the ratio over γ, i.e.,

$$R_{\text{pa}} = e_0 + e_1\gamma + e_2\gamma^2 + e_3\gamma^3 + e_4\gamma^4 + e_5\gamma^5. \tag{31}$$

The model (31) is monotonic over γ and exhibits an NRMSE $<0.001\,\%$ at the integer values of $\gamma \in \Gamma_{\text{red}}$.

C. Reformulation of Gear Dynamics

The integer complexity is further reduced by transforming the non-convex discrete gear dynamics in (8) to the continuous domain, i.e., the gear dynamics is modelled as a continuous state with a discrete control where $\gamma \in [1, \gamma^{\max}]$. Then, the control input u_γ is defined as a binary function [8], [32]

$$u_\gamma(t) = d_{\gamma,\text{up}}(t) - d_{\gamma,\text{dn}}(t), \quad u_\gamma(t) \in \mathbf{U}. \tag{32}$$

To ensure that u_γ still lies in the admissible control set $\mathbf{U}$, an additional constraint is added to the MIOCP as

$$d_{\gamma,\text{up}}(t) + d_{\gamma,\text{dn}}(t) \leq 1, \quad d_{\gamma,\text{dn}}(t), d_{\gamma,\text{dn}}(t) \in \mathbb{B}, \tag{33}$$

where $\mathbb{B} = \{0, 1\}$. The constraint (33) ensures that the binary control function in (32) satisfies the Special Order Set Property (SOS-1) specified in [8], [32]. Such a constraint reduces the admissible set by restricting $u_\gamma^{\min}$ and $u_\gamma^{\max}$ in (9) to values -1 and 1, respectively, which means that the optimizer is only allowed to effect a change of one gear lower or higher at once. Although we present and validate our approaches with such a restricted admissible set, it can be scaled to allow other values for $u_\gamma^{\min}$ and $u_\gamma^{\max}$ stated in (9), by including additional binary variables and combinatorial constraints. For example, to allow change of two gears lower or two gears higher at once, (33) can be replaced with

$$d_{\gamma,\text{up},1}(t) + d_{\gamma,\text{up},2}(t) + d_{\gamma,\text{dn},1}(t) + d_{\gamma,\text{dn},2}(t) \leq 2, \tag{34}$$
$$d_{\gamma,\text{up},1}(t), d_{\gamma,\text{up},2}(t), d_{\gamma,\text{dn},1}(t), d_{\gamma,\text{dn},2}(t) \in \mathbb{B}, \tag{35}$$

apart from the additional combinatorial constraints required to restrict the feasible binary combinations to allowed values.

Notice that, even though the gear ratio is relaxed to a real-valued function and the gear is relaxed to a real value, the gear dynamics in (8) ensure that only integer gears are obtained as long as the problem is initialized with an integer gear and all following gear shifts are integer variables.

D. Relaxation of the Power Balance Constraint

To avoid feasibility issues due to actuator power limitations, the equality constraint (7) is relaxed as

$$P_{\text{ice}}(t) + P_{\text{isg}}(t) \geq P_{\text{s}}(t). \tag{36}$$

This relaxation entails that the net actuator power delivery can be higher than the demand. However, such an allocation is generally avoided by the optimizer, as it results in higher cost. This implies that a strict equality is expected to hold at the solution for all acceleration requests. However, in the braking phase, strict equality of (36) cannot be guaranteed at the solution $\forall t$ due to the effect of dynamics on the ICE braking capacity. This implies that the optimizer allocates or requests less braking power from the actuators (ICE and ISG) than the total demanded power. In such scenarios, the gap in braking power is assumed to be compensated by a friction brake controller that exists in the considered powertrain configuration, but external to the SCC.

E. MPC Implementation of Reformulated MIOCP

Model Predictive Control (MPC) approach is used to implement the SCC energy management problem, as MPC is an effective online control framework to optimize a cost function over a feasible set of constraints for a specific horizon in real-time [5], [41], [42], [47]. The reformulated MIOCP can be represented as

$$z = \min_{x,u} \int_{\zeta}^{\zeta+t_{\text{h}}} \{H_{\text{p}}\left(x, u, \theta, t\right) + W(u,t)\}\, dt \tag{37a}$$
$$\text{s.t.} \quad \dot{P}_{\text{ice}}(t) = f(P_{\text{ice,req}}(t), P_{\text{ice}}(t), \theta(t)), \tag{37b}$$
$$\gamma^{+}(t) = \gamma(t) + d_{\gamma,\text{up}}(t) - d_{\gamma,\text{dn}}(t), \tag{37c}$$
$$x(\zeta) = \hat{x}(\zeta), \tag{37d}$$
$$P_{\text{isg}}(t) \geq P_{\text{s}}(t) - P_{\text{ice}}(t), \tag{37e}$$
$$d_{\gamma,\text{up}}(t) + d_{\gamma,\text{dn}}(t) \leq 1, \tag{37f}$$
$$u^{\min}(\theta(t)) \leq u(t) \leq u^{\max}(\theta(t)), \tag{37g}$$
$$x^{\min}(\theta(t)) \leq x(t) \leq x^{\max}(\theta(t)), \tag{37h}$$
$$\gamma(t) \in [1, \gamma^{\max}], \tag{37i}$$
$$d_{\gamma,\text{up}}(t), d_{\gamma,\text{dn}}(t) \in \mathbb{B}, \tag{37j}$$

where the parameter $\hat{x}(\zeta)$ denotes a vector of initial estimates (guesses) for the states, i.e., $[\hat{\gamma}(\zeta) \quad \hat{P}_{\text{ice}}(\zeta)]^T$. Then, the state $x(t)$, the control $u(t)$ and the input parameter $\theta(t)$ vectors are

$$x(t) = \begin{bmatrix}\gamma(t) & P_{\text{ice}}(t)\end{bmatrix}^T, \tag{38a}$$
$$u(t) = \begin{bmatrix}d_{\gamma,\text{up}}(t) & d_{\gamma,\text{dn}}(t) & P_{\text{ice,req}}(t) & P_{\text{isg}}(t)\end{bmatrix}^T, \tag{38b}$$
$$\theta(t) = \begin{bmatrix}v(t) & \alpha(t) & U_{\text{ocv}}(\zeta) & R_{\text{b}}(\zeta) & \hat{x}^T(\zeta) \\ \lambda_{\text{b}}^*(t) & \lambda_{\text{sr}}(t) & \eta_{\text{ig}}(t) & P_{\text{dm}}(t) & P_{\text{aux}}(t)\end{bmatrix}^T. \tag{38c}$$

The problem is solved for $t \in [\zeta, \zeta + t_{\rm h}]$ and $\zeta \in [t_0, t_{\rm f} - t_{\rm h}]$ where, t_0 and $t_{\rm f}$ represent the start time and the final time of the driving mission, $t_{\rm h}$ refers to the chosen horizon and ζ is the current time of the MPC. As mentioned earlier in Section IV-C, initializing the gear state with an integer value, i.e., $\gamma(\zeta) = \hat{\gamma}(\zeta) \in \Gamma_{\rm red}$, at $\zeta = t_0$, is vital to retain the integer nature of the relaxed gear dynamics in (37c).

F. Transcribing the MIOCP to a Finite Dimensional MINLP

We use direct numerical optimization method, direct multiple shooting [48], to discretize the MIOCP (37) to a finite-dimensional MINLP. This transcription enables exploitation of the problem structure during the solution process [48]. The resulting MINLP is represented as

$$\min_{\tilde{x},\tilde{u}} \; L(\tilde{x}(N+1|j)) + \sum_{k=1}^{N} \phi(\tilde{x}(k|j), \tilde{u}(k|j), \tilde{\theta}(k|j)) \quad (39a)$$

$$\text{s.t.} \quad \tilde{x}(k+1|j) = f(\tilde{x}(k|j), \tilde{u}(k|j), \tilde{\theta}(k|j)), \forall k, \quad (39b)$$

$$\tilde{x}(j|j) = \hat{\tilde{x}}(j), \quad (39c)$$

$$h(\tilde{x}(k|j), \tilde{u}(k|j), \tilde{\theta}(k|j)) \leq 0, \quad \forall k, \quad (39d)$$

$$\tilde{\gamma}(k|j) \in [1, \gamma^{\max}], \quad \forall k, \quad (39e)$$

$$\tilde{d}_{\gamma,l}(k|j) \in \mathbb{B}, \quad l \in \{\text{up}, \text{dn}\}, \quad \forall k, \quad (39f)$$

where the equality (39b) represents the discrete form of dynamics in (37b) and (37c), the inequality (39d) represents the set of inequalities in (37e) to (37h). Similarly, the notation $\tilde{(\cdot)}$ represents the discrete form of vectors in (38), L represents the terminal cost, $\phi(\cdot)$ represents the stage cost at each instant, and $(k|j)$ is the discrete form of continuous time notation, i.e.,

$$(t|\zeta) \longmapsto ((j+k-1)\Delta t | j\Delta t) \longmapsto (k|j) \quad (40)$$

where Δt represents fixed discretization or sampling interval, $k \in \{1, 2, ..., N\}$ refers to the instance within the prediction horizon ($t_{\rm h} \Leftrightarrow N\Delta t$) of N instances, and j refers to the current (or update) instance of MPC in the mission. Subsequently, the problem (39) is solved $\forall j \in \{1, 2, ..., (t_{\rm f}/\Delta t) - N\}$.

Notice that the objective term $\phi(\cdot)$ in (39a) includes the energy cost component (discretized form of Hamiltoninan in (26)) and the gear shift cost component (to penalize frequent gear changes). Furthermore, in problem (39), we use the binary shift control function u_γ as defined in Equations (32) and (33). Consequently, the gear shift cost component becomes a simple function of the binary variables as represented below,

$$w_\gamma(\tilde{d}_{\gamma,\text{up}}(k|j) + \tilde{d}_{\gamma,\text{dn}}(k|j)). \quad (41)$$

V. Numerical Solution Strategies

In this section, we explain the two numerical strategies proposed to approximately solve the finite-dimensional MINLP (39) in a computationally efficient manner.

A. Proposal I: Selective Relaxation Approach (SRA)

In an MPC framework, only the first control action is used among the optimal sequence for the current horizon [48]. Hence, when we solve the problem (39), we only need the first control action to be an integer. We exploit this fact in the SRA strategy and solve a 'selectively-relaxed' MINLP as

$$\min_{\tilde{x},\tilde{u}} \; L(\tilde{x}(N+1|j)) + \sum_{k=1}^{N} \phi(\tilde{x}(k|j), \tilde{u}(k|j), \tilde{\theta}(k|j)) \quad (42a)$$

$$\text{s.t.} \quad \text{(39b) to (39e)}, \quad (42b)$$

$$\tilde{d}_{\gamma,l}(k|j) \in \begin{cases} \mathbb{B} & k = 1, \quad \forall l, \\ [0,1] & k \in \{2, ..., N\}, \quad \forall l, \end{cases} \quad (42c)$$

where $l \in \{\text{up}, \text{dn}\}$. The top case in (42c) shows that the binary constraint is enforced only on the first control action, while the rest of the controls in the current horizon are relaxed within the continuous range between $[0, 1]$. This 'selectively-relaxed' problem can be solved faster compared to problem (39) using off-the-shelf MINLP solvers. To further improve the speed of the solution, in a custom implementation of MINLP solver, problem (42) is decomposed into several subproblems such that an NLP is solved for each integer combination of $\tilde{d}_{\gamma,l}(j|j) \in \mathbb{B}$, $\forall l$ that satisfies (32) and $\tilde{\gamma}(j+1|j) \in \Gamma_{\rm red}$ at each time step j.

B. Proposal II: Round-n-Search Approach (RSA)

The attractive feature of the 'relax-n-round' strategy is the low computational cost, whereas the inability to ensure feasibility is the major limitation of the strategy [32], [33]. This 'relax-n-round' strategy, when applied on (39), induces infeasibility in two cases: i) When the rounded optimal action results in a gear in which the actuators cannot deliver the power demanded in the original problem (39); and ii) When the rounded optimal action results in an infeasible gear in (39), which can occur when the current gear is at or close to the feasible region boundary. We overcome these issues in the proposed RSA strategy by searching the integer feasible space around the solution of the relaxed problem. The motivation is that if the relaxed problem has an optimal and feasible solution, and the integer feasible region of (39) is non-empty, then there exists at least one integer control action ($\exists u_\gamma \in \mathbb{Z}$) around that relaxed solution which is feasible in the MINLP (39). Although theoretical proof to guarantee feasibility of RSA is not provided in this article, the RSA strategy is able to overcome the infeasibility issue faced by known 'relax-n-round' strategies in a simulation study with different drive cycles as explained later in Section VII-F. The RSA is a four-step strategy:

Step 1 - Full Relaxation of the MINLP (FR-MINLP): At time step $j = 1$, the binary constraint on the shift variables (39f) is relaxed to obtain the continuous form of the MINLP (39). This relaxation results in an NLP as

$$\min_{\tilde{x}_{\rm r},\tilde{u}_{\rm r}} \; L(\tilde{x}_{\rm r}(N+1|j)) + \sum_{k=1}^{N} \phi(\tilde{x}_{\rm r}(k|j), \tilde{u}_{\rm r}(k|j), \tilde{\theta}(k|j)) \quad (43a)$$

$$\text{s.t.} \quad \text{(39b) to (39e)}, \quad (43b)$$

$$\tilde{d}_{\gamma,l,{\rm r}}(k|j) \in [0,1], \quad l \in \{\text{up}, \text{dn}\}. \quad (43c)$$

where the vector of relaxed control variables is given by,

$$\tilde{u}_{\rm r} = \begin{bmatrix} \tilde{d}_{\gamma,\text{up,r}} & \tilde{d}_{\gamma,\text{dn,r}} & \tilde{P}_{\text{ice,req}} & \tilde{P}_{\text{isg}} \end{bmatrix}^T, \quad (44)$$

Algorithm 1: Round-n-Search Approach (RSA)

Solution process for update index j and $l \in \{\text{up}, \text{dn}\}$.
Input: Initial estimate $\tilde{u}(k|j)$ or solution $\tilde{u}^*(k|j-1)$, and parameter $\tilde{\theta}(k|j)$, $\forall k$.

Phase-I: Preparation
if $j = 1$ **then**
  Relax integrality constraint, $\tilde{d}_{\gamma,l,\text{r}}(k|j) \in [0,1] \mid \forall l$.
  Compute lower bound solution, $\tilde{u}_\text{r}(k|j)$.
else
  Build an approximation of lower bound solution,

$$\tilde{u}_\text{r}(k|j) = \begin{cases} \tilde{u}^*(k+1|j-1), & k = 1, ..., N-1, \\ \tilde{u}^*(k|j-1), & k = N. \end{cases}$$

end

Phase-II: Solve for integer feasible solution
Compute integer feasible set $U_\text{rsa}(j)$ from $\tilde{u}_\text{r}(j|j)$.
Parameterize the MINLP over $\hat{\tilde{u}}_0$ by fixing the binary controls, i.e., $\tilde{d}_{\gamma,\text{up}}(j|j) - \tilde{d}_{\gamma,\text{dn}}(j|j) = \hat{\tilde{u}}_0$.
Minimize the resulting bi-level NLP to get $\tilde{x}^*, \tilde{u}^*$.
return $\tilde{x}^*(k|j), \tilde{u}^*(k|j), \forall k$

$$\implies \tilde{d}^*_{\gamma,l}(k|j) \in \begin{cases} \mathbb{B} & k = 1, \quad \forall l, \\ [0,1] & k \in \{2, ..., N\}, \quad \forall l. \end{cases}$$

and $\tilde{x}_\text{r}$ represent the state trajectory due to the relaxed control, $\tilde{u}_\text{r}$. This relaxed problem, referred to as FR-MINLP, is solved using an NLP solver to obtain the lower bound solution of (39) for a specific j, i.e., a single MPC update.

Step 2 - Round and Search: The solution of FR-MINLP $\tilde{u}_\text{r}(j|j)$ is used to find the closest integer admissible set $U_\text{rsa}(j)$ for the shift variables in the control vector $\tilde{u}(j|j)$ as

$$\begin{aligned} U_\text{rsa}(j) = \{&\hat{\tilde{u}}_0 \mid \tilde{\gamma}^+(\tilde{\gamma}(j|j), \hat{\tilde{u}}_0) \in \Gamma_\text{red}, \\ &\hat{\tilde{u}}_0 \in \{\lfloor u_{\gamma,r} \rfloor, \lceil u_{\gamma,r} \rceil\}, \ \lfloor u_{\gamma,r} \rfloor, \lceil u_{\gamma,r} \rceil \in \mathbf{U}, \\ &u_{\gamma,r} = \tilde{d}^*_{\gamma,\text{up,r}}(j|j) - \tilde{d}^*_{\gamma,\text{dn,r}}(j|j)\}, \end{aligned} \tag{45}$$

where $\lceil \cdot \rceil$ and $\lfloor \cdot \rfloor$ represent the round-up and round-down operations, respectively. Then the solution for MINLP (39) at time step j is given by the minimizer of the problem

$$[\tilde{x}^*, \tilde{u}^*] = \underset{\tilde{x}(\hat{\tilde{u}}_0), \tilde{u}(\hat{\tilde{u}}_0)}{\arg\min} \quad z_\text{ps}(\tilde{x}, \tilde{u}, \tilde{\theta}, \hat{\tilde{u}}_0), \tag{46a}$$

$$\text{s.t.} \quad (\tilde{x}(\hat{\tilde{u}}_0), \tilde{u}(\hat{\tilde{u}}_0)) \in \pi^*(\hat{\tilde{u}}_0), \ \hat{\tilde{u}}_0 \in U_\text{rsa}(j), \tag{46b}$$

which is a bi-level optimization (parametric NLP) version of MINLP (39) parameterized over $\hat{\tilde{u}}_0$, where the cost $z_\text{ps}(\cdot)$ is

$$L(\tilde{x}(N+1|j)) + \sum_{k=1}^{N} \phi(x(k|j), \tilde{u}(k|j), \tilde{\theta}(k|j), \hat{\tilde{u}}_0), \tag{47}$$

and the implicit policy π^* is a minimizer of the subproblem

$$\pi^*(\hat{\tilde{u}}_0) = \underset{\tilde{x}, \tilde{u}}{\arg\min} \ z_\text{ps}(\tilde{x}, \tilde{u}, \tilde{\theta}, \hat{\tilde{u}}_0), \tag{48a}$$

$$\text{s.t.} \quad \text{(39b) to (39e) and (43c)}, \tag{48b}$$

$$\tilde{d}_{\gamma,\text{up}}(j|j) - \tilde{d}_{\gamma,\text{dn}}(j|j) = \hat{\tilde{u}}_0, \tag{48c}$$

$$\hat{\tilde{u}}_0 \in U_\text{rsa}(j), \tag{48d}$$

Note that the policy $\pi^*(\hat{\tilde{u}}_0)$ has two candidate solutions, one for each $\hat{\tilde{u}}_0 \in U_{RSA}$. Consequently, minimization over the parameter space in problem (46) provides the optimal solution. Furthermore, given the admissible set in (45) is nonempty, the minimization process in (46) ensures the feasibility of the solution of RSA $\forall j$ and the closeness of the solution to the MI optimum. Supportive results are provided in Section VII-F.

Step 3 - Shifting from One Solution to the Next: The predicted control actions in the solution of problem (46), i.e. $\tilde{u}^*(k|j)$ for $k \in \{2, ..., N\}$, are close to the solution at $j+1$. This aspect is further exploited to avoid solving (43) again for the next iterate(s) of the MPC. An approximate solution to the problem (43) at $j+1$ is built by shifting $\tilde{u}^*$ at j as

$$\tilde{u}_\text{r}(k|j+1) = \begin{cases} \tilde{u}^*(k+1|j), & k = 1, ..., N-1, \\ \tilde{u}^*(k|j), & k = N, \end{cases} \tag{49}$$

where the case $\tilde{u}_\text{r}(k|j+1) = \tilde{u}^*(k|j), k = N$, refers to the additional element needed to 'complete' the approximation of the vector of controls.

Step 4 - Repeat 2 and 3: Steps 2 and 3 are repeated, where the built control sequence (49) is used to find the integer admissible set $U_\text{rsa}(j)$ in (45), instead of using the sequence $\tilde{u}^*_\text{r}(j|j)$ of (43), for $j \in \{2, 3, ..., (t_\text{f}/\Delta t) - N\}$.

Furthermore, to solve the original MINLP (39), the control approximation in step 3 reduces the call to an NLP solver by $30\,\% - 45\,\%$ compared to repeating step 1 for $j > 1$. Detailed description of this reduction in computational demand is presented in Section VII-D.

VI. Benchmark Controllers

This section explains the different benchmark controllers that were implemented to obtain reference solutions, which are further used to analyze the performance of the proposed strategies in terms of optimality, effective energy savings, and computational demand in the parallel-HEV.

1) Rule-Based Gear Controller: In this heuristic controller, referred to as BMrk-RB controller, we assume that the TCM uses an experimentally tuned map-based gear shifting algorithm to decide the appropriate gear $\tilde{\gamma}(k|j)$ based on velocity $\tilde{v}(k|j)$ and power demand $\tilde{P}_\text{dm}(k|j)$, since it is a typical approach in production vehicles. Using this shift map, the gear $\tilde{\gamma}(k|j)$ and inturn the angular velocities $\tilde{\omega}_\text{s}(k|j)$, $\tilde{\omega}_\text{ice}(k|j)$ and $\tilde{\omega}_\text{isg}(k|j)$, and the velocity-dependent actuator power limits in (14), (16) and (21) can be estimated for the given mission, prior to optimization. Hence, MINLP (39) is reduced to a much simpler NLP where the objective is to find an optimal control input $\tilde{u}(k|j)$ that allocates the demand between the two actuators while minimizing the overall energy consumption of the HEV. This simplified controller is the exact optimal power-split controller, dy-MPC, proposed in our previous work [40]. The solution of this controller is used as a reference against which the rest of the strategies considered in this study are compared to understand the benefit of co-optimizing the power split and the gear decisions in parallel-HEVs, while considering the ICE dynamics explicitly in the control problem.

TABLE I: Parameter Values of Control-Oriented Models.

Parameter	Value	Parameter	Value
$A_{\rm fa}$	1.92 m^2	$R(\gamma=1)$	5.2500
$c_{\rm ad}$	0.035	$R(\gamma=2)$	3.0288
$c_{\rm rr}$	0.66	$R(\gamma=3)$	1.9500
m	2150 kg	$R(\gamma=4)$	1.4570
g	9.82 m/sec^2	$R(\gamma=5)$	1.2209
$\rho_{\rm air}$	1.18 kg/m^3	$R(\gamma=6)$	1.0000
$r_{\rm wh1}$	0.37 m	$R(\gamma=7)$	0.8086
$J_{\rm wh1}$	3.5 kgm^2	$R(\gamma=8)$	0.6731
$J_{\rm ice}$	0.4 kgm^2	$R_{\rm dg}$	3.1000
$J_{\rm isg}$	0.05 kgm^2	$P_{\rm ice}^{\max}$	257 kW
$\tau_{\rm ice}$	1.25 sec	$\lvert P_{\rm isg}^{\max}\rvert$	35 kW
w_γ	18.00	$\lambda_{\rm b}^*(t)$	2.22 $\forall t$
$\eta_\gamma(\gamma=1:8)$	0.97	Engine idle	900 rpm

2) Dynamic Programming (DP): Among the states in (37), since the gear dynamics (37c) is discrete in nature, we discretize only the continuous ICE dynamics (37b) to solve MIOCP (37) using the DP algorithm, as suggested in [3]. The bounds of the $\tilde{P}_{\rm ice}$ state grid are defined as,

$$\tilde{P}_{\rm ice} \in [\tilde{P}_{\rm ice}^{\min}(\omega_{\rm s}^{\min}), \tilde{P}_{\rm ice}^{\max}(\omega_{\rm s}^{\max})]. \tag{50}$$

The cost criteria is a function of the initial state $\tilde{x}(j|j)$,

$$J^{\rm DP}(\tilde{x}(j|j)) = L(\tilde{x}(N+1|j)) + \sum_{k=1}^{N} \phi^{\rm DP}(\cdot), \tag{51}$$

where $\phi^{\rm DP}(\cdot)$, a function that penalizes both the infeasible state ($\tilde{P}_{\rm ice}$) and the non-admissible controls, is defined as

$$\phi^{\rm DP} = \begin{cases} \phi(\tilde{x}(k|j), \tilde{u}(k|j), \tilde{\theta}(k|j)), & \tilde{x} \in \chi^{\rm d}, \tilde{u} \in \mathbf{U}^{\rm d}, \\ \infty, & \text{otherwise}, \end{cases} \tag{52}$$

where $\chi^{\rm d}$ and $\mathbf{U}^{\rm d}$ denote the feasible region and admissible controls defined by constraints (39d), (39f) and (50). Then the optimal control policy $\tilde{u}^*(\tilde{x}(j|j))$ is found as

$$\tilde{u}^*(\tilde{x}(j|j)) = \underset{\tilde{u}(\tilde{x},k|j)}{\arg\min}\ J^{\rm DP}(\tilde{x}(j|j)). \tag{53}$$

During the solution process, we invert the linear dynamic models in (37b) and (37c) to find the exact control signals, $P_{\rm ice,req}$ and u_γ, required to move between the state grid points. This approach avoids the need for discretization of the control $P_{\rm ice,req}$ and improves the speed of policy estimation. Furthermore, this approach avoids the need for interpolation by choosing the initial state to be exactly at a grid point.

The solution $J^{\rm DP}(\tilde{u}^*)$ is a close approximation to the optimum of MINLP (39). Therefore, the solution $J^{\rm DP}(\tilde{u}^*)$ is used as an effective measure to assess the optimality gap of the solutions obtained using the proposed strategies.

VII. Simulation Results and Discussion

A dynamic simulation of the considered SCC energy management problem was carried out using plant models of the considered HEV platform, described in Section II.

A. Simulation Strategy and Setup

To validate the proposed numerical control strategies, a hybrid approach (refer [1, p. 12] for pictorial representation) was adopted, i.e., a backward simulator is first used to determine the optimal power split and gear choice using predicted information (refer III-A for details on predicted trajectories). These optimal controls are then applied to the forward simulator plants to estimate the actual fuel and energy consumption of the HEV. The forward simulator uses a feedback mechanism to compensate for vehicle speed deviations arising from modelling inaccuracies and powertrain saturation.

The parameter values of the control-oriented models used in this study are provided in Table I. Furthermore, elements of the vector of initial estimate (guesses) $\hat{\tilde{x}}(j)$ are initialized as $\hat{\tilde{\gamma}}(j) = 1$ and $\hat{\tilde{P}}_{\rm ice}(j) = 0$, when $j = 1$. Meanwhile, the other decision variables in the current MPC window are initialized as 0s. All these initial values are chosen to be within the feasible region defined by the constraints (39d) to (39f)). However, when $j \neq 1$, the estimates ($\hat{\tilde{\gamma}}(j)$ and $\hat{\tilde{P}}_{\rm ice}(j)$) of the current states are provided by lower-level controllers as stated in Section III-A. In this case, rest of the decision variables in the horizon are initialized at the predicted values of the previous MPC solution due to their closeness to the solution of the current MPC iterate.

Other configurations and scenarios considered to evaluate the strategies are: i) The solutions of problems (42) and (46), referred to as 'SRA' and 'RSA' respectively, are generated using a custom prototype implementation of the proposed strategies, which inturn calls IPOPT to solve NLP (43) and (48), and the decomposed version of (42); ii) To compare the performance and optimality of the proposed strategies, three additional variants of the HEV were simulated, where two of these variants use controllers BMrk-RB and DP (described in Section VI), respectively, while the third variant uses the FR-MINLP strategy in which (43) is solved for $\forall j$ assuming the transmission to be continuously variable as in (31); iii) To evaluate the integer feasibility of the proposed strategies (RSA and SRA) against the known rounding strategies, the relaxed solution of FR-MINLP is rounded using standard rounding (SR) and sum-up rounding (SUR) strategies stated in [32], [33]. For all the simulations, a discretization interval $\Delta t = 0.5\,\text{sec}$ was used. A prediction horizon $t_{\rm h} = 10\,\text{sec}$ was used to evaluate the solution strategies for the entire mission over multiple MPC updates, while a prediction horizon $t_{\rm h} = t_{\rm f} - t_0$ was used only for single MPC update cases. Furthermore, the time-varying parameter $\lambda_{\rm b}^*(t)$ was optimized offline using methods stated in Remark 1. All simulations were performed on a computer with 32 GB of RAM and an octa-core processor operating at 2.3 GHz.

B. Solutions of the Proposed Strategies (SRA and RSA)

The proposed strategies, SRA and RSA, were evaluated for the WLTC Class-3b drive cycle, and the corresponding solution trajectories are shown in Fig. 6. The primary observation is that the solution, i.e., the state and control trajectories, of both the proposed strategies (SRA and RSA) are exactly the same. Secondly, the proposed strategies did not encounter

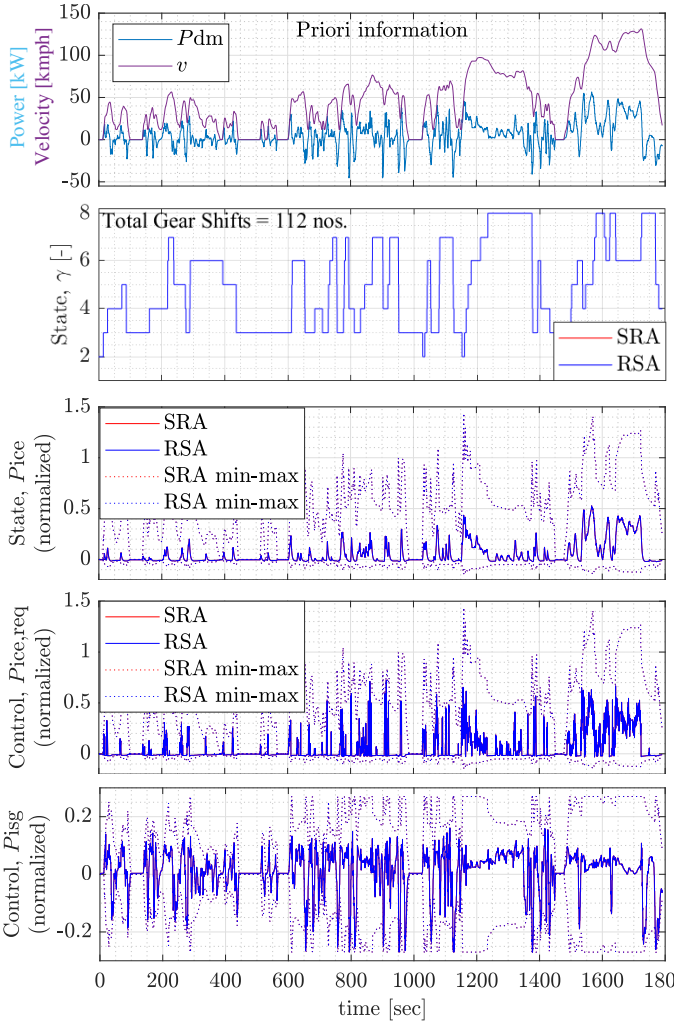
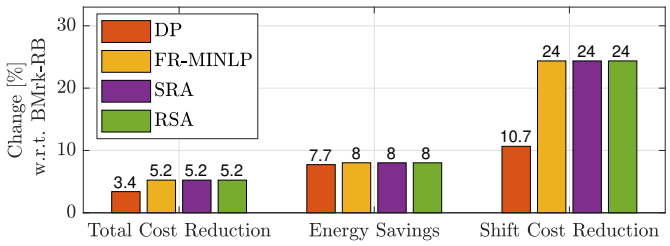
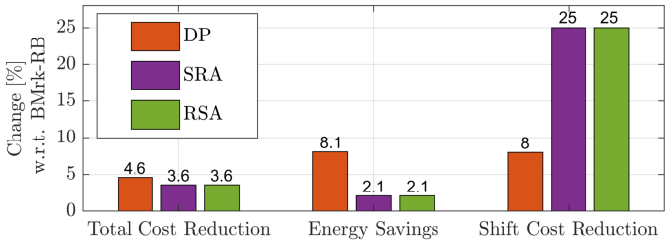


Fig. 6: This figure shows that the solutions of both the proposed strategies, SRA and RSA, are exactly the same, i.e., in the actuator dynamics and the gear trajectories. All the states and control inputs are within bounds. The power in the plots are normalized with a single scaling factor.



(a) This bar graph shows cost comparison over a single MPC update with a prediction horizon $t_{\mathrm{h}} = t_{\mathrm{f}} - t_0$. The solutions of the proposed strategies, SRA and RSA, lie between the solutions of the FR-MINLP (lower bound of (39)) and the DP (upper bound of (39)) strategies, respectively.



(b) This graph shows cost comparison over the entire mission with $t_{\mathrm{h}} = 10\,\mathrm{sec}$. The total cost reduction achieved by both RSA and SRA strategies ($3.6\,\%$) is only less by $1\,\%$ compared to the reduction realized by DP, which shows the closeness of their solution to the global optimum. FR-MINLP solution is neglected as it is not integer feasible.

Fig. 7: Comparison of total cost reduction and its two principal components, energy savings and shift cost reduction, of the evaluated strategies as a relative percentage change w.r.t. the cost of the BMrk-RB strategy.

TABLE II: Reduction in gear changes (improvement of ride comfort) for the entire mission (multiple MPC update case with $t_{\mathrm{h}} = 10\,\mathrm{sec}$)

Control Strategies	Total Gear Shifts	Reduction in gear shifts
BMrk-RB	150 nos.	Reference
DP	138 nos.	8 %
SRA	112 nos.	25 %
RSA	112 nos.	25 %

infeasibility issues during the solution process. Therefore, the solution of RSA and SRA are within their respective min-max limits (feasible region).

Furthermore, both strategies have allocated a higher percentage of propulsive demand to ISG at low vehicle speeds and power demand (around $0\,\mathrm{sec} \leq t \leq 475\,\mathrm{sec}$), where ISG is highly efficient compared to ICE. This allocation to ISG decreases as vehicle speed and power demand increase, to the extent that ICE is widely used to deliver propulsive demand at speeds greater than $90\,\mathrm{kmph}$ and power demand greater than $25\,\mathrm{kW}$. However, both strategies fully exploit the regenerative capacity of the ISG at all speeds. Furthermore, the gear selection is such that the actuator operating speeds are in the range of $900\,\mathrm{rpm}$ to $3300\,\mathrm{rpm}$.

C. Performance Comparison of SRA and RSA Strategies

Fig. 7 shows the comparison of the total cost reduction with its two principal components, energy savings and shift cost reduction, achieved by the evaluated strategies as a relative percentage change w.r.t. the cost incurred by the BMrk-RB strategy. While Fig. 7(a) shows the comparison of cost reduction in a single MPC update with a prediction horizon $t_{\mathrm{h}} = t_{\mathrm{f}} - t_0$, a similar comparison for the entire mission over multiple MPC updates with a prediction horizon of $10\,\mathrm{sec}$ is shown in Fig. 7(b). Furthermore, since the shift cost is a weighted sum of gear changes with w_γ as weight as in (27), the shift cost reduction in Fig. 7(b) correlates exactly with the reduction in the number of gear changes in Table II. However, due to the relaxed nature of the solutions (except DP) in Fig. 7(a), the shift cost reduction of FR-MINLP should be considered an effective upper bound for SRA and RSA.

There are two primary observations from Fig. 7. First, the optimal objective value (the total cost) and the energy savings of the RSA strategy were marginally less ($<0.002\,\%$) than the SRA strategy for both prediction horizon cases, $t_{\mathrm{h}} = 10\,\mathrm{sec}$ and $t_{\mathrm{h}} = t_{\mathrm{f}} - t_0$. Second, as both RSA and SRA strategies have exactly same gear trajectories as their solution, their gear shift costs are same for the penalty considered, w_γ.

Remark 3 (Effect of gear shift penalty w_γ)**.** *When w_γ is*

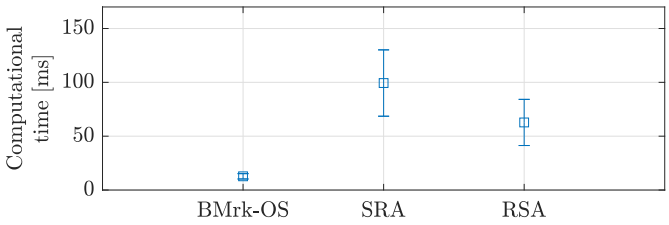


Fig. 8: Box plot showing the computational time statistics for a prototype implementation of few algorithms evaluated conceptually in this study, with $t_{\mathrm{h}} = 10\,\mathrm{sec}$. RSA strategy has a mean computation time of $64\,\mathrm{ms}$, which is $36\,\%$ less than the $100\,\mathrm{ms}$ demanded by SRA. DP demands a mean time of $9890\,\mathrm{ms}$.

reduced by $45\,\%$ the RSA strategy consumes around $2.4\,\%$ more energy but has around $2.5\,\%$ less gear shifts compared to the SRA strategy. Less shifts enhance the attribute 'ride comfort' for the RSA-based HEV.

These observations show that both the proposed strategies perform equally well in terms of the two conflicting performance objectives. These strategies can be further tuned to enhance ride comfort (reducing gear changes) or minimize energy consumption.

D. Computational Demand of SRA and RSA Strategies

From Fig. 8, the RSA strategy shows a considerable reduction in the mean computational load, around $36\,\%$, compared to the SRA strategy. This is due to the fact that RSA solves only two subproblems (i.e., RSA searches for the optimum among two candidate solutions) while SRA solves three subproblems to find an approximate solution to the MINLP (39). Specifically, the RSA strategy minimizes the parametric NLP (46) over two values of $\hat{\tilde{u}}_0$ at each $j > 1$, since the admissible set $U_{\mathrm{rsa}}(j)$ has a maximum of only two integer feasible controls (round-up and round-down values of the relaxed solution) over which (46) is minimized (also recall that the control approximation in step 3 of RSA approach in Section V-B eliminated the need for an additional call to an NLP solver to solve (43) at each $j > 1$ to find the lower bound solution). Whereas, the SRA strategy typically solves a maximum of three subproblems (NLP) resulting from any three binary combinations of candidate control actions $\tilde{d}_{\gamma,l}(j|j) \in \mathbb{B}, \forall l$, at each j to solve (42). Hence, SRA has a higher computational load, whereas RSA performs relatively better. However, both SRA and RSA are about 99 times faster than DP.

Remark 4 (Implementation maturity)**.** *In this article, we have focused on conceptually establishing the practical implications and real-time capabilities of the proposed numerical strategies. Consequently, the computational time statistics shown in Fig. 8 are based only on a prototype implementation of the algorithms considered. Therefore, these results should be seen as a proof-of-concept rather than as a case of benchmarking mature implementation of the algorithms. Furthermore, the order of magnitude of the runtimes in Fig. 8 depicts pessimistic upper bounds for the algorithms, because a mature implementation of these algorithms could be done differently. For example, our prototype implementation in Matlab extensively uses the routines in CasADi [49] and its harness for solver IPOPT [50]. It is quite possible to achieve significant improvements in runtime by using software tailored for real-time MPC implementation with dedicated linear algebra and QP routines like HPIPM [51].*

E. Benefits of Co-Optimization Against BMrk-RB Strategy

To evaluate the benefit of co-optimization strategies in HEVs, we analyze the performance of DP and the proposed strategies against the BMrk-RB strategy, in which we optimize only the power-split decision.

1) Over a Single MPC Update: Fig. 7(a) shows that all co-optimization strategies were able to improve cost reduction, energy savings, and ride comfort, compared to BMrk-RB. Among the co-optimization strategies, DP has the least cost reduction, as its solution is restricted to integer feasible values, unlike the relaxed nature of the problems solved by RSA, SRA and FR-MINLP. Although relaxed solutions appear to have the same cost in Fig. 7(a), the actual cost reduction of SRA and RSA was less than ($<0.009\,\%$) that of FR-MINLP. Such properties of the solutions show that FR-MINLP and DP provide an effective lower and upper bound to the original MINLP (39), respectively, within each MPC update.

2) Over Entire Mission with Multiple MPC Updates: Fig.7(b) shows that all co-optimization strategies were able to achieve $>3.6\,\%$ cost reduction compared to BMrk-RB emphasizing the benefit of co-optimizing power-split and gear selection. The proposed strategies were able to realize around $78\,\%$ of the total cost reduction achieved by DP. Further analysis shows that both SRA and RSA were able to realize only $25\,\%$ energy savings, while they managed about $68\,\%$ more gear shift reduction compared to DP, respectively. Such high energy saving of DP is due to the integer feasibility of its solution throughout the prediction window. Unlike the case of a single MPC update, the relaxed nature of the problem solved by the SRA and RSA strategies results in convergence to local solutions over multiple MPC updates.

Actuator Operating Points Chosen by Co-optimizers: To further understand the impact of co-optimization, the distribution of actuator operating points, i.e., the ICE and ISG power delivery as a function of their angular velocity, is represented as a heat map over the actuator efficiency contours in Fig. 9. Furthermore, the black dashed line (Max. Efficiency) shows the most efficient operating point of the actuator. The main observations in Fig. 9 are: i) The rule-based gear map used in BMrk-RB operates the actuators mainly in the range of $1700\,\mathrm{rpm}$ to $2100\,\mathrm{rpm}$, whereas the co-optimization strategies choose a velocity spread of $900\,\mathrm{rpm}$ to $3300\,\mathrm{rpm}$, by exploiting the additional freedom of gear selection; ii) Unlike BMrk-RB, the co-optimization strategies operate the ICE (the least efficient actuator) at the most efficient operating point possible (relative to the power demand at each time step) which reflects as the hotter region in the ICE operating point distribution (i.e., higher number of instances a specific operating point was chosen) being in parallel with the maximum efficiency line; iii) Similarly, the hotter region in the ISG distribution

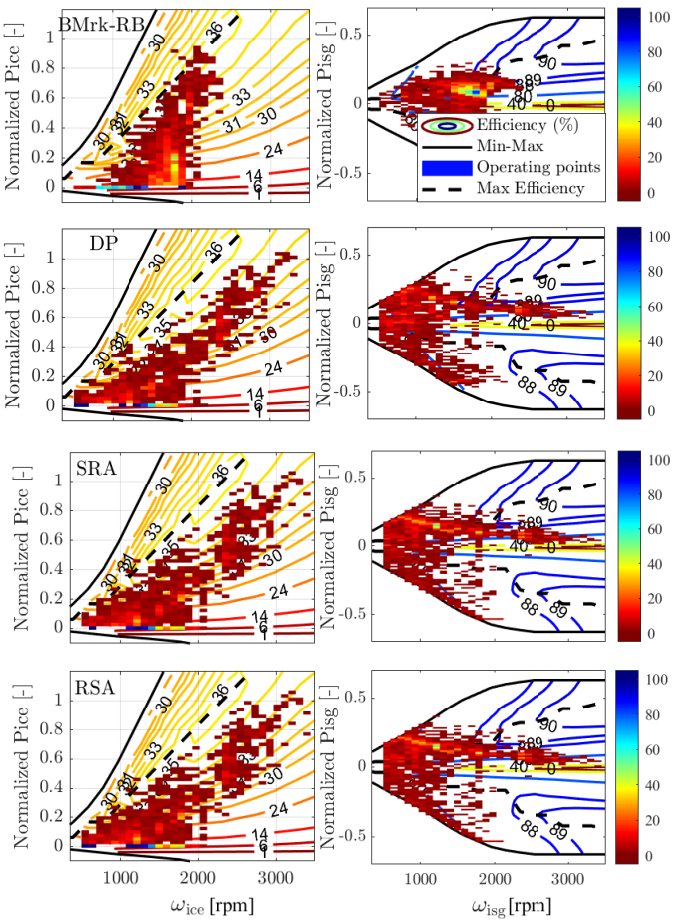


Fig. 9: Distribution of the actuators operating points for the proposed and benchmark strategies. The BMrk-RB strategy operates the actuators mainly in the range of 1700 rpm to 2100 rpm, whereas the co-optimization strategies choose a wider spread of 900 rpm to 3300 rpm by exploiting the additional freedom of gear selection. The co-optimization strategies frequently chose operating points that are close and parallel to the maximum efficiency line (w.r.t. the operating speed) resulting in energy savings of $2.1\,\% - 8.1\,\%$ compared to BMrk-RB. In the colorbar used, the numerical values 0 and 100 represent the minimum and the maximum number of instances an operating point was chosen by the control strategy. Subsequently, these values indicate the cold and hot regions in the heatmap, respectively.

shows that the co-optimization strategies allocate most of the power demand to the ISG at low speeds where the ICE is the least efficient and then gradually shift the load to the ICE as the speed increases.

Effect of Co-state on Operating Point Selection: The considered co-state parameter λ_b (translates into a unit cost of battery energy) has a considerable impact on actuator allocation and gear selection. For example, the hot spot of the operating speed range moves toward the high-speed region, as well as the percentage of propulsive demand allocated to the ICE increases as λ_b increases, as shown in Fig. 10. Furthermore, since λ_b used in Fig. 10 is sufficiently high (3 times the λ_b used in Fig. 9), the allocation is such that ICE is used to charge the battery (ISG in generation mode) in addition to delivering the entire or a large part of propulsive demand. Moreover, the hot spots of the ICE operating points are closer to the maximum efficiency line in Fig. 10 compared to Fig. 9.

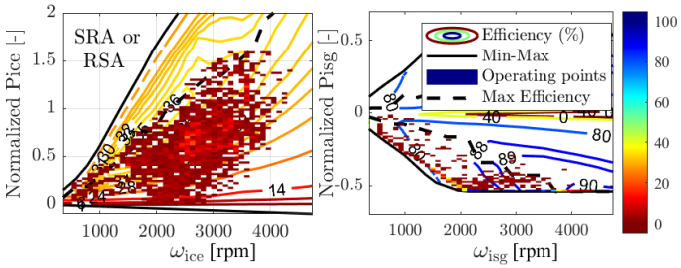


Fig. 10: Actuator operating point distribution of the proposed strategies with $3\lambda_b$, i.e., 3 times the value of co-state used to obtain the results in Fig. 9. The hot-spot (colors in the range between red and orange) of the ICE operating points are now closer to the maximum efficiency line and are grouped at higher speeds (around 3000 rpm), compared to the values in Fig. 9. The ICE delivers entire or major part of the propulsive demand whereas the ISG is either in generation or regeneration mode.

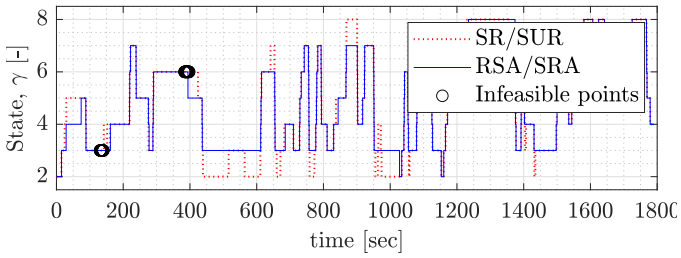


Fig. 11: Plot showing the infeasibility issue in known standard rounding (SR) and sum-up rounding (SUR) strategies [32], [33] against the proposed strategies, under WLTC Class-3b drive cycle. Blue solid line shows the gear trajectory for RSA and SRA strategies whereas the red dotted line shows the trajectory for the known rounding strategies being compared. Black circles around 140 sec and 390 sec show the instances where the usage of SR and SUR resulted in infeasible gear values in which the actuators were not able to deliver the demanded power. Notice that at these instances the proposed strategies have chosen a gear lower than the rounding strategies to ensure feasibility of the solution.

These observations show the superiority of co-optimization strategies (DP, SRA and RSA) as they realize around $2.1\,\% - 8.1\,\%$ energy savings compared to BMrk-RB, by exploiting the additional control freedom of gear selection.

F. Feasibility of Proposed Strategies Against Known Relax-N-Round (Rounding) Strategies

Fig.7(b) shows that the proposed strategies, RSA and SRA, managed to find a feasible integer solution for (39) which is within $1\,\%$ of the DP solution. However, when the relaxed solution of FR-MINLP was rounded using known strategies such as standard rounding (SR) and sum-up rounding (SUR) stated in [32], [33], its resulting solution is not integer feasible

TABLE III: Feasibility of RSA and SRA against known rounding strategies.

Drive Cycle	SRA / RSA Strategy	Rounding Strategies (SR / SUR) [32], [33]
WLTC (Class 3b)	Feasible	Infeasible
CADC (Urban)	Feasible	Infeasible
CADC (Rural Road)	Feasible	Infeasible
CADC (Motor Way)	Feasible	Infeasible
US06-SFTP	Feasible	Infeasible

in the original problem (39). Therefore, the solution of FR-MINLP is not included in Fig.7(b).

To further confirm this observation of improvement in solution feasibility, the proposed strategies were evaluated against known rounding strategies (SR and SUR) for additional drive cycles like Common Artemis Driving Cycles (CADC) and US06 - Supplemental Federal Test Procedure (US06-SFTP). The corresponding results in Table III show that both RSA and SRA managed to find a feasible integer solution for (39) while the known rounding strategies suffer from infeasibility for the drive cycles considered. These results support the feasibility argument proposed in Section V-B. For example, the reason for the infeasibility of the known rounding strategies is that the rounded control action resulted in a gear in which the actuators were not able to deliver the demanded power in (39), as shown in Fig.11 for the WLTC Class-3b drive cycle. This issue is overcome by the proposed RSA strategy due to the presence of the re-optimization process after the rounding action (Step 2 in Section V-B), which searches for feasible integer value around the relaxed solution. Whereas, in SRA, the 'selective relaxation' enforced by constraint (42c) ensures that the first control action in each MPC horizon is, in fact, integer feasible.

G. Optimality of the Solution and the Effect of Horizon

To evaluate the optimality of the proposed strategies, RSA and SRA, we intend that the solutions of FR-MINLP and DP provide the respective lower and upper bounds for (39). However, from Figs. 7(b) and 9 it is observed that DP provides a closest approximation of the optimum of (39), due to the integer nature of its solution. However, the solution of FR-MINLP (z_{r}^{*}) is infeasible in the original problem (39). Therefore, it is not obvious how to quantify the exact optimality gap of the solutions of the RSA and SRA strategies without knowing a lower bound solution. However, since the difference in the total cost reduction achieved by the proposed strategies and the DP is within $1\,\%$, the solutions of both RSA and SRA are considered to be rather close to the optimum.

Furthermore, the above observations in the optimality of the solutions of DP and FR-MINLP contradict that in Fig. 7(a) where FR-MINLP and DP provide an effective lower and upper bound, respectively, to (39) over a single MPC update. This contradiction is due to the difference in the horizon size in both cases. This shows that more studies are required to understand the effect of the horizon and realize the maximum potential of the proposed strategies.

H. Sensitivity of the Solution to Initial Estimates (Guesses)

As stated in Section VII-A, only the initial guesses for the decision variables at the start of the mission ($j = 1$) can be chosen. Therefore, its choice can affect the convergence to the solution. For all other time steps ($j \neq 1$), the MPC controller uses the current state estimates from the lower-level controllers and the predicted values from the immediate previous solution as an initial guess for the remaining decision variables in each MPC update. Since we used the previous solution at the time steps $j \neq 1$, the trajectory of the solution for the entire mission is sensitive only to the initial guess at the first time step $j = 1$.

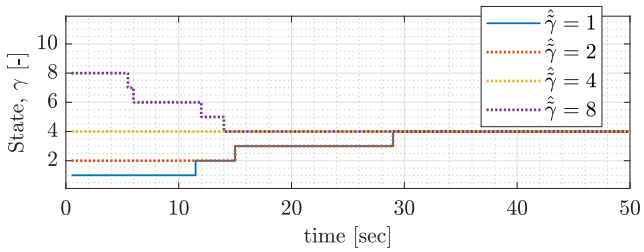


Fig. 12: Plot showing the effect of different initial guesses $\hat{\hat{x}}(j)$ on gear state evolution. For the feasible initial guesses shown, the resulting trajectories converge to the same solution despite the initial differences. Other decision variables were initialized with a feasible value during the evaluation.

To understand the effect of this first initial guess on the solution of the proposed strategies under WLTC Class 3b cycle, different feasible values were evaluated as initial guesses for the decision variables in the problem (39), at $j = 1$. Among them, the initial guess $\hat{\hat{\gamma}}(j)$ of the gear state showed a noticeable difference in the solutions of the proposed strategies and is therefore presented in Fig. 12 while ignoring the rest.

Fig. 12, shows the variation in the evolution of the gear-state trajectory during the first $50\,\mathrm{sec}$ of the WLTC Class 3b cycle, when the problem (39) was solved for different values of $\hat{\hat{\gamma}}(j)$ while initializing the other decision variables to any fixed feasible value at $j = 1$. All trajectories converge to the same solution in a few time steps, despite differences in the feasible initial guesses considered. Although the initial difference in the solutions resulted in a marginal variation in total gear shifts, in the range of $110\,\mathrm{nos}$ to $114\,\mathrm{nos}$, the variations in total cost and energy savings were negligible ($<0.001\,\%$).

VIII. Conclusion

In this paper, the energy management problem of co-optimizing the gear and power-split is formulated as an MIOCP by explicitly including the continuous dynamics of ICE and the discrete dynamics of gear (transmission). Then, numerical relaxations and reformulations of the MIOCP are proposed to reduce the computational demand of the solution process. Two numerical solution strategies, the Selective Relaxation Approach (SRA) and the Round-n-Search Approach (RSA), are proposed to approximately solve an MINLP, the transcribed version of the MIOCP. The proposed strategies are then evaluated against benchmark strategies based on rule-based gear selection and DP, on an HEV simulation platform.

The results show that the proposed co-optimization strategies, RSA and SRA, show superior performance with a cost reduction of around $3.6\,\%$ compared to the rule-based gear selection strategy commonly used in production vehicles. This shows the benefit of co-optimizing gear selection with the power-split decision while considering the actuator dynamics explicitly in the optimization. Among the proposed strategies, the RSA strategy shows a reduction of around $35\,\%$ in the mean computation time compared to the SRA strategy. However, both proposed strategies perform equally well in terms of conflicting performance objectives, as their cost difference is negligible ($<0.002\,\%$). In addition, both strategies can be further tuned to enhance ride comfort (reducing gear changes) or minimize energy consumption.

Furthermore, both proposed strategies show superior performance in terms of integer feasibility, i.e., both SRA and RSA were able to overcome the infeasibilities encountered by known rounding strategies under different drive cycles. Furthermore, the cost reduction achieved by both RSA and SRA ($3.6\,\%$) is only less by $1\,\%$ compared to the reduction realized by DP, while remaining 99 times faster than DP. This shows the computational benefit of the proposed strategies and the closeness of their solutions to the optimum.

These results show that simple relaxation-based numerical solution strategies are an efficient method to solve the mixed integer optimal control problem in real-time on an online (or embedded) controller in electrified automotive applications. Furthermore, these proposed mixed-integer solution strategies can be extended and integrated into a computer software in future intelligent transportation systems to solve similar MI problems, including charge point selection for electric vehicles, fleet management, intelligent traffic management, and a wide range of other mobility solutions.

As part of future work, understanding the effect of factors like unique shift penalty for each strategy (or replacing penalty with a hard constraint on number of gear changes), horizon size, parameter variations, and prediction inaccuracies, on optimality and computational demand is vital to maximize the potential of the proposed strategies in a real world application. Importantly, more work is needed on theoretical guarantees for the feasibility and expected optimality gap. In addition, evaluating the proposed strategies against approaches like ADMM-based [15], [39], combinatorial integral approximation decomposition [32], [33], [52], [53], iterative [9], [34], [35] and others [36], [37] is of key interest. Furthermore, we intend to consider variations in actuator capability (similar to [54]) and improve the maturity of implementation of the proposed strategies to evaluate their performance in a concept vehicle in the near future.

ACKNOWLEDGMENT

The authors would like to thank the Sweden´s Innovation Agency (Vinnova), the Volvo Car Corporation, and the Chalmers University of Technology for support.

REFERENCES

[1] S. Onori, L. Serrao, and G. Rizzoni, *Hybrid Electric Vehicles: Energy Management Strategies*. No. 2192-6786 in SpringerBriefs in Control, Automation and Robotics, London: Springer-Verlag, 1 ed., 2016.

[2] M. Montazeri-Gh, Z. Pourbafarani, and M. Mahmoodi-k, "Comparative study of different types of PHEV optimal control strategies in real-world conditions," *Proceedings of the Institution of Mechanical Engineers, Part D: Journal of Automobile Engineering*, vol. 232, pp. 1597–1610, Oct. 2018. Publisher: IMECHE.

[3] L. Guzzella and A. Sciarretta, *Vehicle Propulsion Systems*. Springer-Verlag Berlin Heidelberg, 3 ed., 2013.

[4] O. Sundström, *Optimal control and design of hybrid-electric vehicles*. Doctoral Thesis, ETH Zurich, 2009. https://doi.org/10.3929/ethz-a-005902040.

[5] P. Pisu and G. Rizzoni, "A Comparative Study Of Supervisory Control Strategies for Hybrid Electric Vehicles," *IEEE Transactions on Control Systems Technology*, vol. 15, pp. 506–518, May 2007.

[6] A. Sciarretta and L. Guzzella, "Control of hybrid electric vehicles," *IEEE Control Systems Magazine*, vol. 27, pp. 60–70, Apr. 2007.

[7] IEA(2019), "Global EV Outlook 2019," tech. rep., IEA, Paris. https://www.iea.org/reports/global-ev-outlook-2019.

[8] M. Joševski and D. Abel, "Gear shifting and engine on/off optimal control in hybrid electric vehicles using partial outer convexification," in *2016 IEEE Conference on Control Applications (CCA)*, pp. 562–568, Sept. 2016.

[9] N. Murgovski, B. Egardt, and M. Nilsson, "Cooperative energy management of automated vehicles," *Control Engineering Practice*, vol. 57, pp. 84–98, Dec. 2016.

[10] L. Schmitt, M. Keller, T. Albin, and D. Abel, "Real-Time Nonlinear Model Predictive Control for the Energy Management of Hybrid Electric Vehicles in a Hierarchical Framework," in *2020 American Control Conference (ACC)*, pp. 1961–1967, July 2020.

[11] N. Murgovski, L. Johannesson, J. Sjöberg, and B. Egardt, "Component sizing of a plug-in hybrid electric powertrain via convex optimization," *Mechatronics*, vol. 22, pp. 106–120, Feb. 2012.

[12] A. Sciarretta, G. De Nunzio, and L. L. Ojeda, "Optimal Ecodriving Control: Energy-Efficient Driving of Road Vehicles as an Optimal Control Problem," *IEEE Control Systems Magazine*, vol. 35, pp. 71–90, Oct. 2015.

[13] L. Johannesson, N. Murgovski, E. Jonasson, J. Hellgren, and B. Egardt, "Predictive energy management of hybrid long-haul trucks," *Control Engineering Practice*, vol. 41, pp. 83–97, Aug. 2015.

[14] V. Ngo, T. Hofman, M. Steinbuch, and A. Serrarens, "Optimal Control of the Gearshift Command for Hybrid Electric Vehicles," *IEEE Transactions on Vehicular Technology*, vol. 61, pp. 3531–3543, Oct. 2012.

[15] R. Takapoui, N. Moehle, S. Boyd, and A. Bemporad, "A simple effective heuristic for embedded mixed-integer quadratic programming," *International Journal of Control*, vol. 93, pp. 2–12, Jan. 2020.

[16] D. Ambühl, *Energy management strategies for hybrid electric vehicles*. Doctoral Thesis, ETH Zurich, 2009. https://doi.org/10.3929/ethz-a-005902053.

[17] C.-C. Lin, J.-M. Kang, J. Grizzle, and H. Peng, "Energy management strategy for a parallel hybrid electric truck," in *Proceedings of the 2001 American Control Conference. (Cat. No.01CH37148)*, vol. 4, pp. 2878–2883, June 2001.

[18] R. Bellman, "Dynamic Programming," *Science*, vol. 153, no. 3731, pp. 34–37, 1966. Publisher: American Association for the Advancement of Science.

[19] J. Lee and S. Leyffer, eds., *Mixed Integer Nonlinear Programming*, vol. 154 of *The IMA Volumes in Mathematics and its Applications*. New York, NY: Springer New York, 1 ed., 2012.

[20] N. V. Sahinidis, "Mixed-integer nonlinear programming 2018," *Optimization and Engineering*, vol. 20, pp. 301–306, June 2019.

[21] P. Belotti, C. Kirches, S. Leyffer, J. Linderoth, J. Luedtke, and A. Mahajan, "Mixed-integer nonlinear optimization*†," *Acta Numerica*, vol. 22, pp. 1–131, May 2013. Publisher: Cambridge University Press.

[22] V. van Reeven, T. Hofman, R. Huisman, and M. Steinbuch, "Extending Energy Management in Hybrid Electric Vehicles with explicit control of gear shifting and start-stop," in *2012 American Control Conference (ACC)*, pp. 521–526, June 2012.

[23] N. Robuschi, C. Zeile, S. Sager, and F. Braghin, "Multiphase mixed-integer nonlinear optimal control of hybrid electric vehicles," *Automatica*, vol. 123, p. 109325, Jan. 2021.

[24] P. Bonami, A. Olivares, M. Soler, and E. Staffetti, "Multiphase Mixed-Integer Optimal Control Approach to Aircraft Trajectory Optimization," *Journal of Guidance, Control, and Dynamics*, Sept. 2013. Publisher: American Institute of Aeronautics and Astronautics.

[25] R. T. Meyer, M. Žefran, and R. A. DeCarlo, "A Comparison of the Embedding Method With Multiparametric Programming, Mixed-Integer Programming, Gradient-Descent, and Hybrid Minimum Principle-Based Methods," *IEEE Transactions on Control Systems Technology*, vol. 22, pp. 1784–1800, Sept. 2014.

[26] K. Han, N. Li, I. Kolmanovsky, A. Girard, Y. Wang, D. Filev, and E. Dai, "Hierarchical Optimization of Speed and Gearshift Control for Battery Electric Vehicles Using Preview Information," in *2020 American Control Conference (ACC)*, pp. 4913–4919, July 2020.

[27] F. M. Hante and S. Sager, "Relaxation Methods for Mixed-Integer Optimal Control of Partial Differential Equations," *Computational Optimization and Applications*, vol. 55, pp. 197–225, May 2013.

[28] H. Yu, F. Zhang, J. Xi, and D. Cao, "Mixed-Integer Optimal Design and Energy Management of Hybrid Electric Vehicles With Automated Manual Transmissions," *IEEE Transactions on Vehicular Technology*, vol. 69, pp. 12705–12715, Nov. 2020.

[29] C. Zeile, N. Robuschi, and S. Sager, "Mixed-integer optimal control under minimum dwell time constraints," *Mathematical Programming*, vol. 188, pp. 653–694, Aug. 2021.

[30] G. Li and D. Görges, "Energy management strategy for parallel hybrid electric vehicles based on approximate dynamic programming and

velocity forecast," *Journal of the Franklin Institute*, vol. 356, pp. 9502–9523, Nov. 2019.
[31] J. Ritzmann, A. Christon, M. Salazar, and C. Onder, "Fuel-Optimal Power Split and Gear Selection Strategies for a Hybrid Electric Vehicle," in *14th International Conference on Engines & Vehicles*, SAE Technical Paper 2019-24-0205, 2019. https://doi.org/10.4271/2019-24-0205.
[32] C. Kirches, *Fast Numerical Methods for Mixed-Integer Nonlinear Model-Predictive Control*. Wiesbaden: Vieweg+Teubner Verlag, Springer, 1st ed., 2011. https://doi.org/10.1007/978-3-8348-8202-8.
[33] S. Sager, *Numerical methods for mixed–integer optimal control problems*. Der Andere Verlag, Dec. 2005.
[34] M. Joševski and D. Abel, "Distributed predictive control approach for fuel efficient gear shifting in hybrid electric vehicles," in *2016 European Control Conference (ECC)*, pp. 2366–2373, June 2016.
[35] N. Robuschi, M. Salazar, N. Viscera, F. Braghin, and C. H. Onder, "Minimum-Fuel Energy Management of a Hybrid Electric Vehicle via Iterative Linear Programming," *IEEE Transactions on Vehicular Technology*, vol. 69, pp. 14575–14587, Dec. 2020.
[36] N. Li, K. Han, I. Kolmanovsky, and A. Girard, "Coordinated Receding-Horizon Control of Battery Electric Vehicle Speed and Gearshift Using Relaxed Mixed-Integer Nonlinear Programming," *IEEE Transactions on Control Systems Technology*, vol. 30, pp. 1473–1483, Sept. 2021. https://doi.org/10.1109/TCST.2021.3111538.
[37] Q. Zhou and C. Du, "A two-term energy management strategy of hybrid electric vehicles for power distribution and gear selection with intelligent state-of-charge reference," *Journal of Energy Storage*, vol. 42, p. 103054, Oct. 2021.
[38] S. Gros and M. Zanon, "Reinforcement Learning for mixed-integer problems based on MPC," *IFAC-PapersOnLine*, vol. 53, pp. 5219–5224, Jan. 2020.
[39] S. East and M. Cannon, "Fast Optimal Energy Management With Engine On/Off Decisions for Plug-in Hybrid Electric Vehicles," *IEEE Control Systems Letters*, vol. 3, pp. 1074–1079, Oct. 2019.
[40] A. Ganesan, S. Gros, N. Murgovski, C. F. Lee, and M. Sivertsson, "Effect of Engine Dynamics on Optimal Power-Split Control Strategies in Hybrid Electric Vehicles," in *2020 IEEE Vehicle Power and Propulsion Conference (VPPC)*, (Gijon, Spain), pp. 1–8, IEEE, Nov. 2020.
[41] F. Yan, J. Wang, and K. Huang, "Hybrid Electric Vehicle Model Predictive Control Torque-Split Strategy Incorporating Engine Transient Characteristics," *IEEE Transactions on Vehicular Technology*, vol. 61, pp. 2458–2467, July 2012.
[42] M. Bidarvatan and M. Shahbakhti, "Analysis and Control of Torque Split in Hybrid Electric Vehicles by Incorporating Powertrain Dynamics," *Journal of Dynamic Systems, Measurement, and Control*, vol. 140, Nov. 2018.
[43] C. J. Oglieve, M. Mohammadpour, and H. Rahnejat, "Optimisation of the vehicle transmission and the gear-shifting strategy for the minimum fuel consumption and the minimum nitrogen oxide emissions," *Proceedings of the Institution of Mechanical Engineers, Part D: Journal of Automobile Engineering*, vol. 231, pp. 883–899, June 2017.
[44] Y. Wang, C. Zhang, and Z. Chen, "Model-based State-of-energy Estimation of Lithium-ion Batteries in Electric Vehicles," *Energy Procedia*, vol. 88, pp. 998–1004, June 2016.
[45] N. Kim, S. Cha, and H. Peng, "Optimal Control of Hybrid Electric Vehicles Based on Pontryagin's Minimum Principle," *IEEE Transactions on Control Systems Technology*, vol. 19, pp. 1279–1287, Sept. 2011.
[46] F. Zhang, K. Xu, C. Zhou, S. Han, H. Pang, and Y. Cui, "Predictive Equivalent Consumption Minimization Strategy for Hybrid Electric Vehicles," in *2019 IEEE Vehicle Power and Propulsion Conference (VPPC)*, pp. 1–5, Oct. 2019.
[47] N. Murgovski, L. Johannesson, J. Hellgren, B. Egardt, and J. Sjöberg, "Convex Optimization of Charging Infrastructure Design and Component Sizing of a Plug-in Series HEV Powertrain," *IFAC Proceedings Volumes*, vol. 44, pp. 13052–13057, Jan. 2011.
[48] M. Diehl and S. Gros, *Numerical Optimal Control*. Optimization in Engineering Center (OPTEC), 2017-draft ed., 2011.
[49] J. A. E. Andersson, J. Gillis, G. Horn, J. B. Rawlings, and M. Diehl, "CasADi: a software framework for nonlinear optimization and optimal control," *Mathematical Programming Computation*, vol. 11, pp. 1–36, Mar. 2019.
[50] A. Wächter and L. T. Biegler, "On the implementation of an interior-point filter line-search algorithm for large-scale nonlinear programming," *Mathematical Programming*, vol. 106, pp. 25–57, Mar. 2006.
[51] G. Frison and M. Diehl, "HPIPM: a high-performance quadratic programming framework for model predictive control," *IFAC-PapersOnLine*, vol. 53, no. 2, pp. 6563–6569, 2020.
[52] S. Sager, M. Jung, and C. Kirches, "Combinatorial integral approximation," *Mathematical Methods of Operations Research*, vol. 73, p. 363, Apr. 2011.
[53] S. C. Bengea and R. A. DeCarlo, "Optimal control of switching systems," *Automatica*, vol. 41, pp. 11–27, Jan. 2005.
[54] C. Yang, M. Zha, W. Wang, L. Yang, S. You, and C. Xiang, "Motor-Temperature-Aware Predictive Energy Management Strategy for Plug-In Hybrid Electric Vehicles Using Rolling Game Optimization," *IEEE Transactions on Transportation Electrification*, vol. 7, pp. 2209–2223, Dec. 2021.



Anand Ganesan received the M.S. degree in energy and power engineering from the University of Warwick, Coventry, UK, in 2016. As part of the Volvo Cars Industrial Ph.D. program (VIPP), he is currently pursuing a Ph.D. degree in systems and control at Chalmers University of Technology, Gothenburg, Sweden. He also holds a research position at the R&D department of Volvo Cars, Gothenburg, Sweden. His research work is in the area of vehicle energy and motion control, with a focus on computationally efficient numerical methods for mixed-integer optimal control problems in electrified vehicles.



Sébastien Gros received his Ph.D. degree from EPFL, Switzerland, in 2007. After a journey by bicycle from Switzerland to the Everest base camp in full autonomy, he joined a R&D group hosted at Strathclyde University focusing on wind turbine control. In 2011, he joined the University of KU Leuven, where his main research focus was on optimal control and fast MPC for complex mechanical systems. He joined the Department of Signals and Systems at Chalmers University of Technology, Göteborg in 2013, where he became Associate Professor in 2017. He is now a full professor at the Dept. of Eng. Cybernetics, NTNU, Norway, and Guest Prof. at Chalmers. His main research interests include numerical methods, real-time optimal control, reinforcement learning, and optimal control of energy-related applications.



Nikolce Murgovski received the M.S. degree in software engineering from University West, Trollhättan, Sweden, in 2007, and the M.S. degree in applied physics and the Ph.D. degree in systems and control from Chalmers University of Technology, Gothenburg, Sweden, in 2007 and 2012, respectively. He is currently an Associate Professor in the Department of Electrical Engineering at Chalmers University of Technology. His research interests include modelling and simulation of dynamic systems and their use in problems of optimal plant design and control. His typical research projects are in electromobility, autonomous driving, and active safety in automobiles.